

Validation of Satellite Lifetime Predictions at Leonid Space

Rev 1.1, authored 2026-04-10 by Scott Shambaugh

leonidspace.com/contact

Executive Summary

Leonid Space provides real-time satellite lifetime predictions for low Earth orbit missions. This report validates our prediction pipeline through comprehensive backtesting against 934 satellites that deorbited between 1961 and 2024, demonstrating operational readiness for commercial deployment.

Methodology

We backtested against previously deorbited non-maneuvering objects (debris, rocket bodies, and unknown), using TLE data from Space-Track and space weather records spanning six solar cycles. We simulated the final year of flight, and compared predicted deorbit dates against actuals. Our three-stage validation approach progressively removed hindsight to arrive at fully predictive operational conditions.

Key Results

This is the first large-scale validation of lifetime predictions using forecasted space weather – all other studies have done so on small sets of satellites, with the benefit of space weather hindsight, or for short-horizon reentry events. For well-characterized satellites in known conditions, we show **4x improvement in accuracy over ESA’s state-of-the-art DRAMA & DISCOS tooling**, and **8x improvement over NASA’s DAS**.

Scenario	Space Weather	Ballistic Coefficient	1-Year Accuracy
Perfect Knowledge	Known	Extracted	6.0 days (1.6%)
Historical Conditions	Known	Estimated	18.6 days (5.1%)
Fully Predictive	Forecasted	Estimated	45.5 days (12.4%)

We show that after drag coefficient estimation, **solar cycle forecasting dominates all other error sources** and higher fidelity propagators or atmosphere models are of low importance. Our approach measures the uncertainty inherent in each scenario and calibrates our Monte Carlo forecasts such that all output variance is captured in the predicted distribution and **no additional uncertainty needs to be added**.

Performance

Our custom semianalytic propagator executes over 340x faster than a reference Orekit implementation, enabling rapid Monte Carlo analysis across large satellite populations. In comparison against other propagation software using identical inputs, Leonid's predictions show equivalent or better accuracy at a 55x speedup versus ESA's DRAMA, and a 9x speedup versus NASA’s DAS.

Implications

These results establish a performance baseline for Leonid's lifetime prediction services. The demonstrated accuracy supports mission planning, regulatory compliance, and operational decision-making for LEO satellite operators facing an increasingly dynamic atmospheric environment.

Document History

Revision / DOI	Prepared By	Software version	Changes	Published
Rev. 1.0 arXiv:2601.02453v1	Scott Shambaugh	1.0.1	-	2026-01-05
Rev. 1.1 (this document)	Scott Shambaugh	1.4.0	<ul style="list-style-type: none"> Faster custom and Orekit propagator metrics NASA DAS accuracy comparison added 	2026-04-10

Motivation

Space weather has upended the crowded environment of low Earth orbit. Densities in LEO this solar cycle have been 2-3x higher than the pre-cycle scientific consensus prediction, invalidating the lifetime assumptions in current business cases and national security missions [1]. Many satellite operators have reported dramatic impacts to their constellations as a direct result of drag:

- SpaceX lost a full launch of Starlink Satellites in 2022 during a solar storm. [2]
- Capella Space lost 6 Whitney satellites after the stronger-than-expected solar cycle cut their lifetime expectations from 3 years to 9 months. [1]
- Planet Labs implemented new low drag modes and added ballast weight to their Dove satellites to combat higher than expected drag. [3]
- Binar Space lost 3 satellites only 2 months after launch, expecting an 8-9 month mission. [4]
- NASA's 4 TROPICS hurricane monitoring satellites reentered in 2025, 2.5 years into a planned 9-year and recently expected 5-6-year mission. [5]

Leonid Space was started at the beginning of 2025 to address this critical data gap in LEO operations. We provide real-time satellite monitoring and lifetime estimation services for satellite operators, regulators, and space domain awareness partners. Our lifetime prediction software leverages on-orbit data and the latest space weather predictions to produce insights. We enable operators to weather the storm and accurately predict revenue, plan production schedules, and ensure mission continuity.

The real proof of a prediction is in how well it matches reality. We prove ours through a comprehensive backtesting campaign of 934 deorbited satellites, by showing that our pipeline can recreate their last year of flight. We start with the benefit of hindsight and use the actual TLE and space weather data from that year to show accuracy in a "perfect knowledge" scenario. Then through two more steps we arrive at a fully predictive scenario that mimics the realistic operational scenario of evaluating currently flying spacecraft. These probabilistic forecasts are scored, and we end up at a measure of our prediction accuracy.

Notice: This document is informational. Forecasts and models herein are probabilistic and may be inaccurate for individual objects or time periods.

Processing Pipeline

This report validates the lifetime prediction software that forms the core of Leonid’s business. It is made up from several pieces that work together in a combined pipeline: a custom high-speed orbit propagator, automatic ballistic coefficient estimation from on-orbit data, space weather forecasts from NASA, and robust Monte Carlo analysis capabilities. We will explain each of these components in turn.

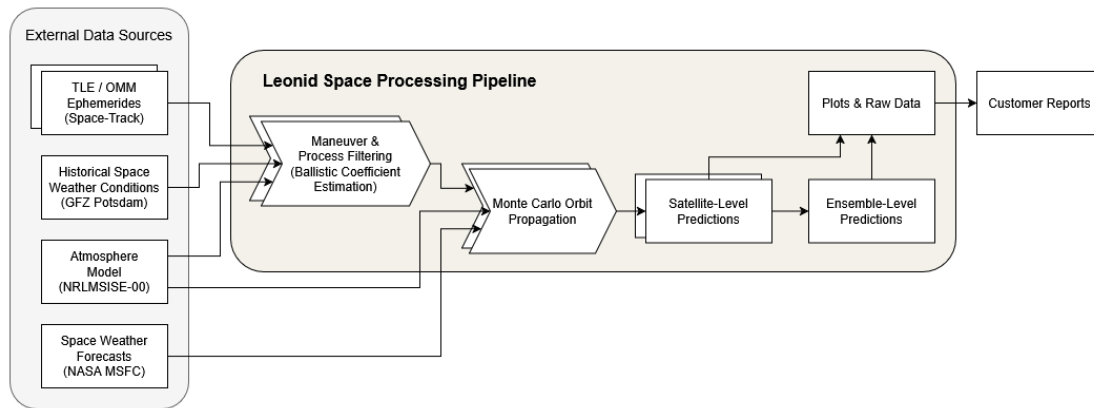


Figure 1: Diagram of the processing pipeline for Leonid’s satellite lifetime prediction software.

Orbit Propagation

Propagation Approach

Orbit propagation is performed with custom in-house software that uses a semianalytic approach based on [6], [7], and [8], which propagates mean elements for an eccentric orbit under the effects of atmospheric drag and the J2 term of an oblate planet. We extended these references in two ways. First, we model a co-rotating atmosphere rather than a static one. Second, we calculate densities along each orbit using NRLMSISE-00 with specified space weather conditions. The full equations of motion and their derivations are omitted from this document but are available for commercial partners to review.

This approach strikes a balance between speed and orbit propagation accuracy. Analytical approaches like [7] which assume a constant density atmosphere or others which assume an exponential atmosphere can avoid integrating drag forces by using analytic approximations. But the atmosphere cannot be assumed to be so static. Even in constant space weather conditions, solar heating effects result in 5x density variation between the day and night side of the Earth at LEO altitudes. Capturing these significant spatial and temporal variations in density is critical for accurate drag modeling, and we believe that for real-world applications there is no substitute for direct calculation and integration.

Solar radiation pressure (SRP) is ignored as a first-order force for lifetime propagation in LEO’s drag-dominated environment. The omission of SRP is common in satellite lifetime analysis and will be justified by the accuracy of the “perfect knowledge” propagation results, but future work will investigate computationally efficient means of adding this to the force modeling for highly eccentric orbits.

The most computationally expensive part of the propagation is calculating the densities. For days-long integration periods needed for e.g. conjunction analysis, full numerical propagation with a small timestep and many density model calls is feasible. But for lifetime analysis where the integration period can be years to decades long, this semianalytic approach with reduced forces, mean elements, and quadrature

integration over an orbit is necessary. Note also that higher fidelity modeling would not necessarily give any better results. As we show later, over these longer timescales space weather uncertainty dwarfs all other sources of error.

Atmosphere Model

There are a number of high altitude atmosphere models available to use, and good comparisons between them can be found in [9], [10], [11], and [12]. The driving use of atmosphere models in the space industry today is for conjunction screening, for which the relevant timescale is hours to days. As a result, the dimension along which most of these models compete is in capturing high-fidelity short-timescale dynamics. But they all offer similar performance over quiescent periods and longer timeframes, with the analysis in [12] showing near equivalent performance between top models over timescales as short as 48 hours. The comparisons in [13] and [14] found only a 0.1% spread between several models for reentry timing accuracy over a 28 day horizon. Even during solar storm events, drag spikes occur over a period of only a few hours and so the highest-fidelity density modeling is not necessary to accurately predict lifetime when integrating over weeks to months to years. Long term bias factors between models exist, but this is implicitly corrected for by using the same model for historical C_B estimation and future propagation (see the discussion of debiasing via “effective density” in [12]).

For our purposes then, the most important factors in atmosphere model selection are scientific acceptance, fast runtime, open licensing of the model and its space weather input data, and availability of input data for the whole of satellite tracking history. We use the NRLMSISE-00 model via the *pymis* library [15] which wraps the original FORTRAN code [16].

Implementation

Starting from initial conditions supplied manually or extracted from two-line elements (TLEs), the mean elements are propagated using the equations of motion. Element perturbations are evaluated to orbit-average values with Gauss-Legendre quadrature, and the space weather conditions at each timestep are combined with the satellite position at each quadrature point to find the corresponding atmospheric densities ρ . Successive integration steps forward in time are taken via a Runge-Kutta method, with an adaptive timestep conditioned against the rate of altitude decay. For payload operators, the implementation supports propulsive orbit control with delta-V applied at each step according to propulsion system characteristics and target orbit elements, but the validation campaign here only tests against non-propulsive free-flying objects. Uncertain parameters can be dispersed, and Monte Carlo simulations are executed using the *monaco* library [17]. We use cloud-based parallel processing to rapidly simulate ensemble forecasts.

Propagator Validation

This propagator was compared against a Python-wrapped Orekit implementation configured with a DSST (Draper Semianalytic Satellite Theory) propagator using J_2 and drag forces, a co-rotating NRLMSISE-00 atmosphere, constant space weather conditions, and a Dormand Prince 8(5,3) integrator [18] [19]. We checked a representative test case of a satellite with $C_B=0.033$ flying during F10.7=180 and $A_p=4$ space weather conditions in a 480x620 km, 51.5 deg mid-inclination orbit over a 365 day integration period. Our propagator took 0.070 seconds to run on a laptop versus 23.7 seconds for Orekit (a 340x speedup), and the final semi-major axis matched to within 2.0 km. This good agreement shows that our orbit-averaged

quadrature approach reproduces DSST drag evolution with orders-of-magnitude faster computation, making it suitable for long-duration lifetime and Monte-Carlo analyses.

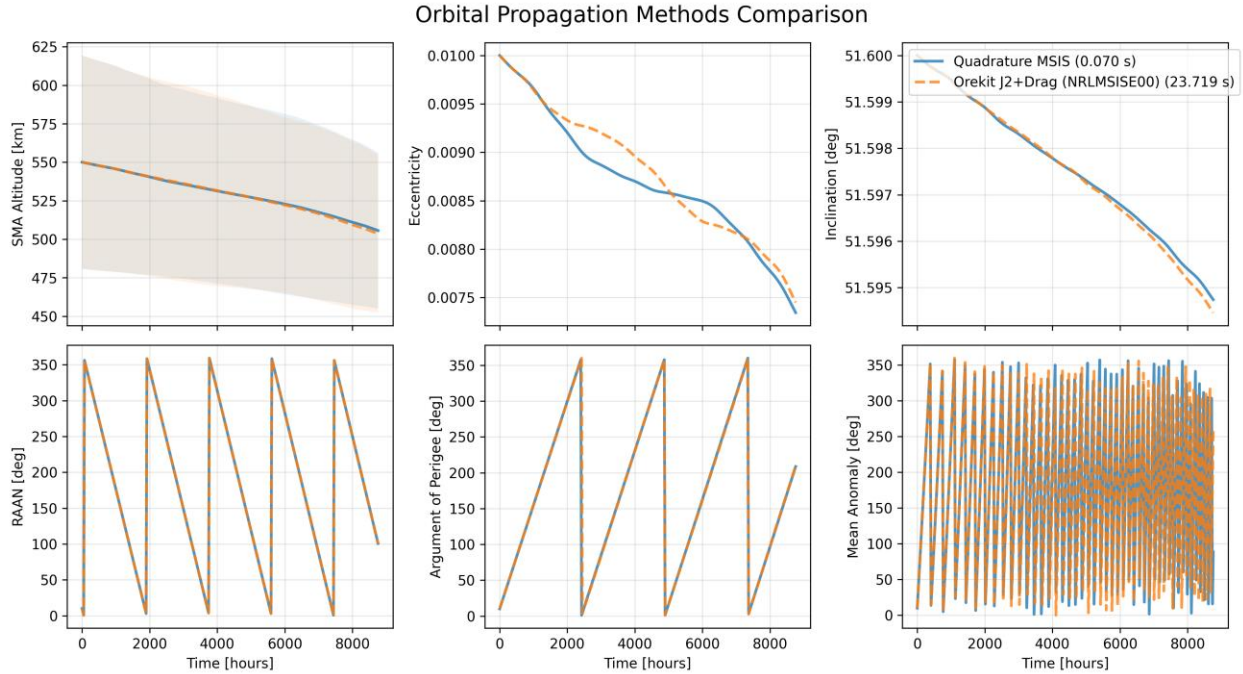


Figure 2: Leonid’s custom propagator vs Orekit’s DSST with J2 and a co-rotating NRLMSISE-00 atmosphere. Shaded region in SMA panel shows perigee-apogee altitude range. Note the one-day timestep aliases the mean anomaly.

We also show alignment to ESA’s DRAMA and NASA’s DAS propagation results later in this report.

Ballistic Coefficient Estimation

The ballistic coefficient C_B as a function of satellite coefficient of drag C_D , mass m , and frontal area A is defined as $C_B = C_D A / m$; note that some sources use the reciprocal of this definition.

TLE BSTAR Parameter

The BSTAR term in TLEs notionally defines the drag component of spacecraft motion, and can be converted to C_B via the equation below. A common pitfall for new astrodynamists who are not familiar with warnings such as in [20], is that this is a fitted parameter within the SGP4 model that “soaks up” all non-modeled forces, and may bear little relation to realistic C_B estimates for drag modeling. However there are few published examples that show just how bad this conversion is (see one in section 9.4.1 in [21]). This will be demonstrated later.

$$C_B = \frac{2 * BSTAR}{R_{Earth} \rho_0}$$

$$R_{Earth} = 6375.135 \text{ km} \quad \rho_0 = 2.461 * 10^{-5} \text{ kg/m}^3$$

Instantaneous C_B Extraction from TLEs

With drag as the dominant nonconservative force in LEO, we can extract C_B from the change in orbital momentum L . Between each pair of successive TLEs, the satellite state is propagated from the first to

second epoch using the *skyfield* SGP4 propagator at a small timestep [22]. The atmospheric density at each timestep is calculated using the resulting state vectors and space weather conditions, and averaged to give the average density during that flight regime $\bar{\rho}$. This is combined with the averaged squared airspeed $\overline{v_{rel}^2}$ and acceleration f_{drag} extracted from the change in momentum at the given semi-major axis a to estimate the ballistic coefficient. This is similar in approach to [23], [24], [25], [26], and [27].

$$L = r \times v$$

$$f_{drag} = \frac{1}{a} \frac{d|L|}{dt}$$

$$C_B = -\frac{2f_{drag}}{\bar{\rho} \overline{v_{rel}^2}}$$

Maneuver & Process Filtering

The resulting C_B time history is a noisy signal. This is a result of both process and measurement noise sources, denoted below with (P) and (M). The good news for lifetime analysis is that only a few of these noise sources are expected to not be stationary processes when integrated over long timescales. Those which are generally non-stationary and may significantly bias results are marked as (P*) and (M*).

1. (P) Changes in frontal area and coefficient of drag of the satellite as it reorients its attitude relative to the airstream.
2. (P*) Changes in area or mass as the satellite deploys structures or burns propellant.
3. (P*) Long-term changes in orbital operations (e.g. a switch to “high drag” mode such as has been demonstrated by SpaceX, Capella Space, and Planet).
4. (P) Higher order variations in atmospheric density not captured by the NRLMSISE-00 model.
5. (P) Higher order variation in atmospheric wind beyond the co-rotation assumption.
6. (P) Shorter timescale and higher order variations in space weather drivers such as Kp or F10.7.
7. (P*) Orbital maneuvers using on-board thrusters.
8. (P) Unmodeled forces such as aerodynamic lift, Solar & Earth radiation pressure, Sun & Moon third body gravitational effects, electromagnetic drag, and higher order Earth gravitational harmonics.
9. (M) TLE generation artifacts and SGP4 assumptions.
10. (M) Inherent tracking uncertainty & gross measurement errors from ground-based radar systems.
11. (M) Lack of cross-calibration between ground-based radar systems.
12. (M*) Cross-tagging of space objects.
13. (M) Calculation assumptions such as timestep quantization, integration scheme, etc.

For this validation campaign payloads are explicitly excluded, so the only expected non-stationary perturbation is from cross-tagging of space objects. This is rare – manual review of outlier lifetime prediction cases found only three debris objects which had a large persistent change in orbital elements which might indicate permanent cross-tagging (NORAD IDs 6345, 6352, 12754).

For payloads, deployment of structures generally happens immediately after launch and does not impact results. Change in propellant mass is generally a small fraction of overall mass, especially after initial orbit acquisition burns. Long-term operational changes need to be detected from pattern-of-life analysis and

are not covered here. Leonid’s maneuver detection algorithms will be discussed and validated in a follow-on report.

After maneuver detection and exclusion, determining C_B from the noisy trace turns into a physically-grounded signal processing problem. Figure 3 below shows a representative trace which highlights several of the practical issues encountered: high-amplitude measurement noise which manifests both continuously over medium-duration time periods and as short duration spikes, long-duration and medium-duration (especially from the Sun’s 27-day Carrington rotational period) process drift, highly variable timesteps, and non-physical C_B values. Leonid’s approach to solving this problem is considered proprietary, and only our results will be presented here.

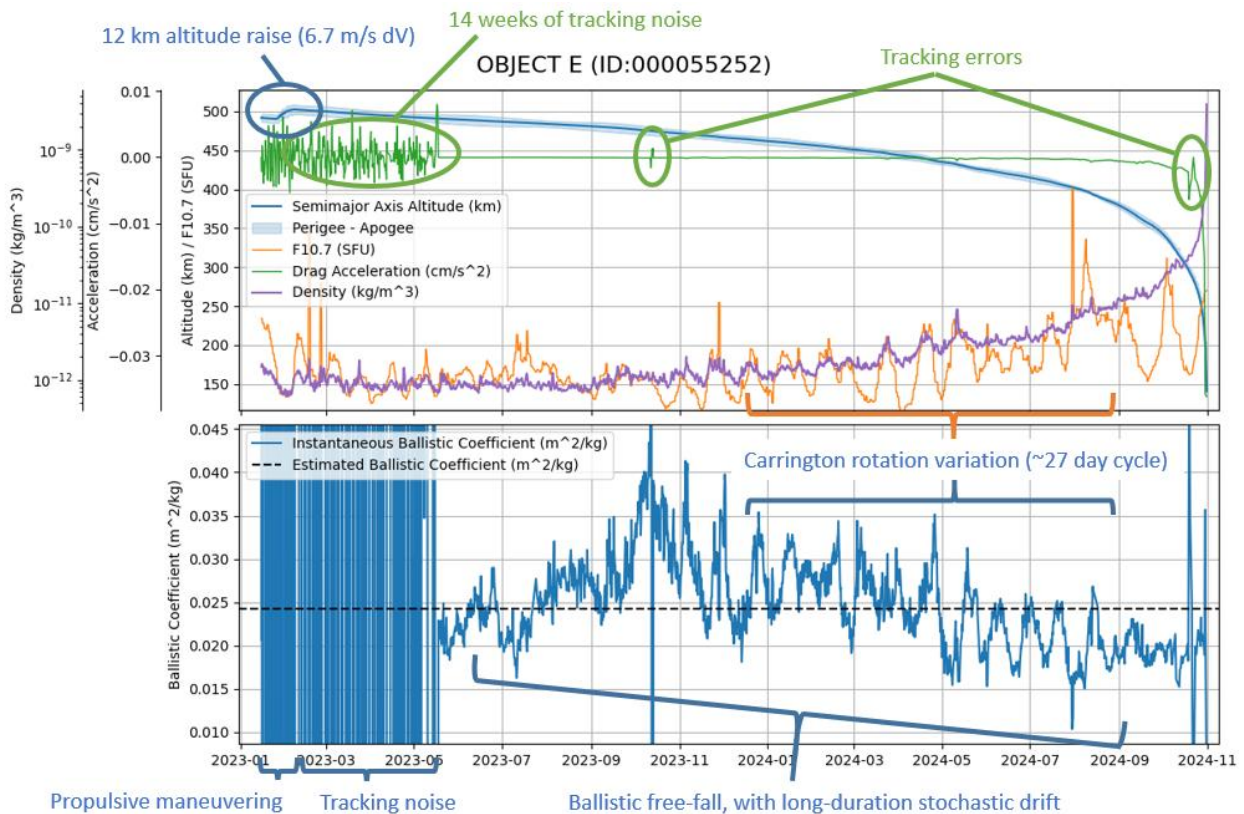


Figure 3: Processed orbital data for NORAD ID 55252 “Object E” / “Jilin-1 Mofang-02A-03”. Top plot shows semimajor axis altitude (blue), F10.7 solar flux (orange), acceleration extracted from TLEs (green), and average atmospheric density seen by the spacecraft in each time interval (purple). The bottom plot shows the instantaneous C_B and its estimated value for future propagation.

In this case NORAD ID 55252 “Object E” is classified as “Unknown” in space-track.org’s SATCAT database, however Celestrak [28] identifies it as Jilin-1 Mofang-02A-03, a Chinese commercial Earth-imaging satellite. No public information on its propulsive capabilities is available, however our analysis shows that its semi-major axis increases by 12 km raise shortly after deployment, followed by a period of high tracking noise, and finally a ballistic free-fall trajectory with minimal tracking noise.

Validation Approach

Scenario

We will backtest Leonid’s deorbit predictions against a large dataset of past deorbit events. Using orbit data from space-track.org’s TLEs [29], we will attempt to predict the date of deorbit starting from the satellite state one year prior to reentry. One year is chosen as an easily interpretable long-duration benchmark, with the hypothesis that prediction error will scale proportionally to different durations. This is consistent with prior backtesting studies that report relative (duration-normalized) lifetime error, and that outlier error is driven by lifetimes that extend over multiple solar cycles [30]. Backtesting against other timeframes to validate this proposition will be explored in follow-on investigations.

For this analysis, deorbit is defined as the date when a satellite’s semi-major axis falls below 300 km altitude. Below this altitude tracking data becomes sparse, so ground truth reference data is often not available. And this is an operationally-relevant threshold – at this point most objects have only a few days before they hit ~80km altitude and burn up. Predicting the precise timing or location of the reentry event is not a goal of this software.

Dispersed Monte Carlo analysis is performed by multiplying the combined quantity $\rho C_D A/m$ over time by a fixed scale factor s to capture the inherent process noise. For a chosen drag dispersion d , the scale factor for each case is chosen from the log-uniform distribution $s_i \sim \text{LogUniform}((1+d)^{-1}, 1+d)$, which ensures multiplicative symmetry around 1. We ran one $s_0 = 1$ nominal case and $n = 20$ dispersed cases for each satellite – enough to build a distribution while keeping computational runtime for many iterations over the whole ensemble reasonable.

Scoring

The differences between the one-year true remaining lifetime for each satellite and the deorbit time for each case forms the set of prediction errors, where positive error means that the satellite deorbited earlier than predicted. The median error of all samples is calculated for each satellite as a measure of the prediction bias. The prediction accuracy is measured using an empirical continuously ranked probability score (CRPS) from the set of errors. Both the median error and CRPS calculations for a single satellite are bootstrapped 100 times from the sample distribution, and their averages are the primary quality metrics. The CRPS can be thought of as a generalization of the mean absolute error for probabilistic forecasts, and for a single non-dispersed prediction is equivalent to the absolute error.

If we have the set of predicted deorbit dates $x \in \{x_1, \dots, x_n\}$ and the true deorbit date y , then the CRPS value for each satellite is calculated as below. Over the whole ensemble of m satellites, we look at the median of the CRPS values and median errors to score the run.

$$CRPS = \frac{1}{n} \sum_{i=1}^n |x_i - y| - \frac{1}{2n^2} \sum_{i=1}^n \sum_{j=1}^n |x_i - x_j|$$

Additionally, we score the dispersed predictions by calculating the rank percentile of each true deorbit date within the set of predictions for each satellite. This is bootstrapped as well. We then look at the ensemble of rank percentiles for all satellites and compare this distribution to an ideal uniform distribution, which we can plot as a histogram or a calibration curve of its empirical cumulative distribution function (ECDF). This is scored using the Cramér-von Mises (CvM) criterion, which measures the integrated

squared difference between the ECDF and the straight-line CDF of the uniform distribution. The CvM doesn't have a physical interpretation, but lets us compare the relative accuracy of dispersed predictions. The equations below show the formulas, where p_k is the rank percentile of the true deorbit date for the k^{th} satellite and $p_{(1)} \leq \dots \leq p_{(m)}$ are those values when sorted. Percentiles below 0.5 indicate that our simulations predicted a longer lifespan than reality.

$$p_k = \text{count}\{x_{k,i} \leq y_k\}/n$$

$$CvM = \frac{1}{12m} + \sum_{k=1}^m \left(p_{(k)} - \frac{2k-1}{2m} \right)^2$$

Validation Process

Validation will proceed in three steps. At each step the dispersion parameter will be tuned to minimize the CvM score, which will characterize the inherent uncertainty in that configuration.

1. **Perfect Knowledge:** Simulate with actual space weather data and C_B extracted from the last year of flight. This validates the end-to-end software toolchain and its ability to reproduce satellite deorbit dates versus ground truth on-orbit data. The uncertainty here characterizes the temporal variation in C_B due to all unmodeled process and measurement noise.
2. **Historical Conditions:** Simulate with actual space weather data and C_B estimated from the 30 days prior to simulation start. This validates extrapolating drag parameters into the future.
3. **Fully Predictive:** Simulate with forecasted space weather data and C_B estimated from the 30 days prior to simulation start. This is analogous to a deorbit analysis performed on a spacecraft flying today, and the additional uncertainty relative to step 2 is entirely due to the unpredictability of future space weather conditions.

Satellite Test Set

Satellite Selection Criteria

A large test set of satellites in LEO that had deorbited due to ballistic freefall was needed. While the deorbit software can account for orbit control maneuvers using onboard propulsion systems, this requires information about orbit control plans and propulsive capabilities from operators that is not generally publicly available. For this reason, all "PAYLOAD" objects were excluded from this analysis. Some "UNKNOWN" objects may be active spacecraft with maneuvering capabilities, but we don't see their impact in the results.

The entire historical SATCAT catalog (~66,000 objects) was analyzed to find a large set of candidate objects which could be used to validate lifetime predictions. The following filters were applied to find a set of 4,730 candidate objects:

1. OBJECT_TYPE equal to one of "DEBRIS", "ROCKET BODY", "UNKNOWN", or "OTHER". This excludes "PAYLOAD" objects.
2. RCS_SIZE not equal to "SMALL", to exclude objects with a $< 0.1 \text{ m}^2$ radar cross section (RCS) in an effort to reduce measurement noise.
3. DECAY date prior to 2025-01-01T00:00:00Z.

4. At least 1 year and 90 days between LAUNCH and DECAY dates.

These 4,730 candidate objects were further downselected to 934 satellites in LEO by processing their TLEs and applying the following filters:

5. TLE data exists in space-track.org’s bulk historical archive.
6. Perigee and apogee altitudes for the initial TLE between 80 and 2000 km altitude.
7. Semi-major axis altitude for the initial TLE higher than 300 km.
8. Perigee altitude for the final TLE before deorbit lower than 500 km.

Test Set Characteristics

Figure 4 below shows the semi-major axis traces of all 934 satellites in the test set. The full historical timespan of human space activity is well covered, starting from when large-scale radar tracking began in 1961 with the operationalization of the first Space Fence.

The effects of solar cycle are apparent with the characteristic “stairstep” pattern of steeper decay during solar maxima and flatter decay during solar minima. The resulting clustering of deorbit events during solar maxima means that the majority of the validation analysis happens during these higher-density periods of time, although the test set is large enough that there is still good coverage during the lower-density solar minima. Note also that data cuts off below 200 km – at this altitude most objects are falling fast enough to have only hours before they hit the thick portion of the atmosphere at 80 km and burn up.

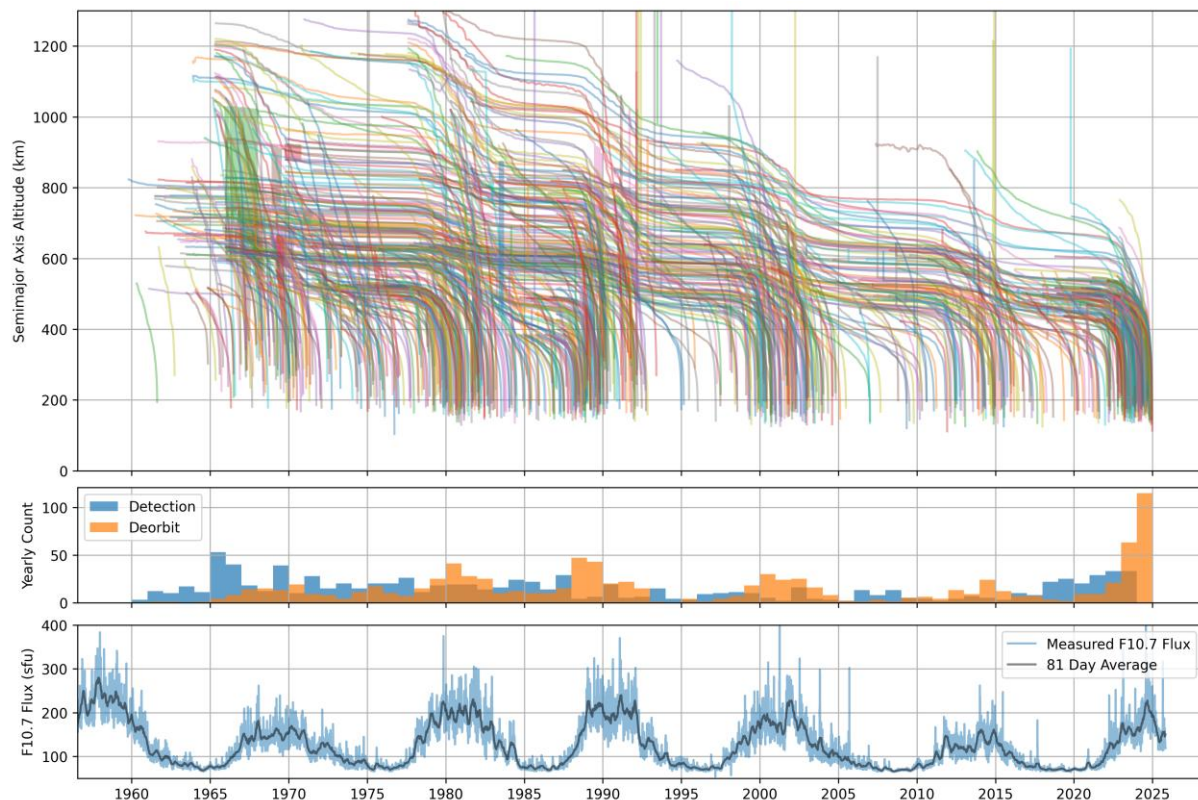


Figure 4: Semi-major axis altitude traces for the test set of 934 LEO spacecraft (top), yearly counts of when the objects were detected and deorbited (middle), and the historical F10.7 solar flux (bottom).

Figure 5 below show the initial orbit eccentricity and inclination distribution for the test set, as well as the counts for each radar cross-section and object type categories. We see good coverage of all these parameters.

With the initial orbits restricted to between 80 and 2000 km altitude, this implies a maximum eccentricity of 0.129. The highest eccentricity in the test set belongs to object 20358 “SL-12 R/B(AUX MOTOR)” with its initial orbit of 226x1991 km giving it an eccentricity of 0.118. It also has the highest inclination at 151 deg. “MEDIUM” objects have a radar cross-sectional area between 0.1 m² and 1.0 m², and “LARGE” objects are > 1.0 m². No objects were labeled with the “OTHER” type.

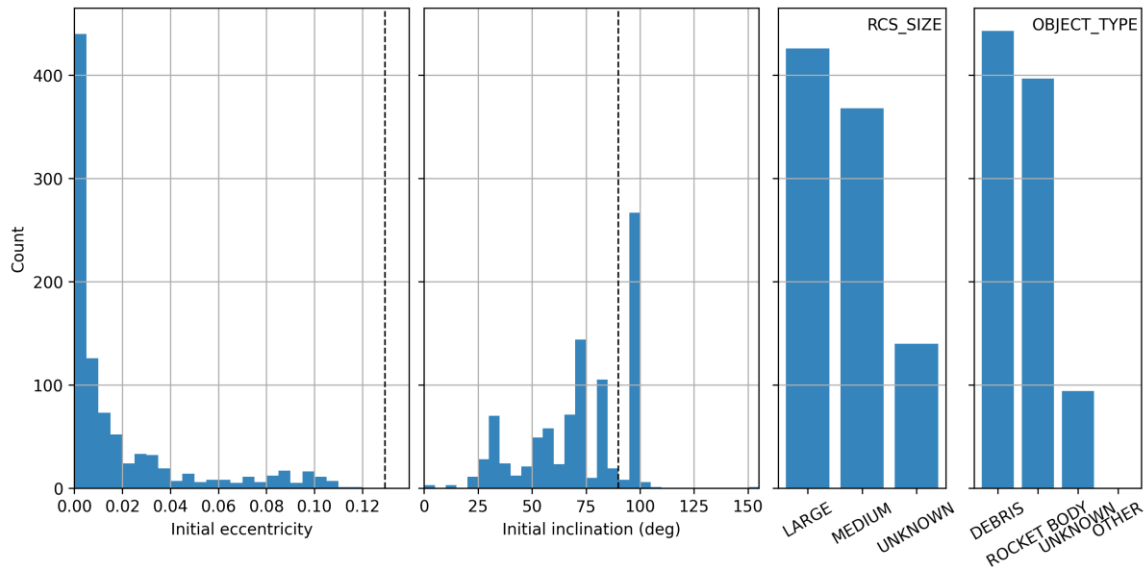


Figure 5: Characteristics of the test set of 934 LEO spacecraft. Initial eccentricity with maximum possible eccentricity of 0.129 marked (left), initial inclination with purely polar orbit of 90 deg marked (middle left), radar cross-section category (middle right), and object type category (right).

Space Weather

The NRLMSISE-00 atmosphere model uses F10.7 solar flux and the geomagnetic Ap indices as the driving space weather inputs to its density calculations. These are both obtained from the datafiles published by Geomagnetic Observatory Niemegek, GFZ Helmholtz Centre for Geosciences [31].

For solar cycle predictions, we use the forecasts published by NASA’s Marshall Space Flight Center (MSFC), which have been continuously published monthly since March 1999 [32] [33]. It uses a modified McNish-Lincoln method to predict out one solar cycle into the future (currently through 2042) [34]. We can disperse this by calculating a standard deviation from the 5th and 95th percentile forecasts in the datafiles, and assuming a normal distribution. For purely predictive historical backtesting, we use the most recent contemporary forecast that was available at each satellite’s simulation start date.

Other forecasts are available, such the one released by NOAA’s Space Weather Prediction Center’s (SWPC’s) [35]. However this forecast was recently overhauled in 2025 and does not have a collection of contemporary historical forecasts to backtest with.

For dates beyond MSFC’s predictions, we use the 13-month smoothed historical average cycle and can disperse high or low based on the historical standard deviation of all stacked historical cycles. A notional

average Ap index of 14 is used for future dates past 2042. Future work will look at quantifying variation and modeling solar cycle predictions on shorter temporal timescales, which [36] shows is influential to lifetime predictions.

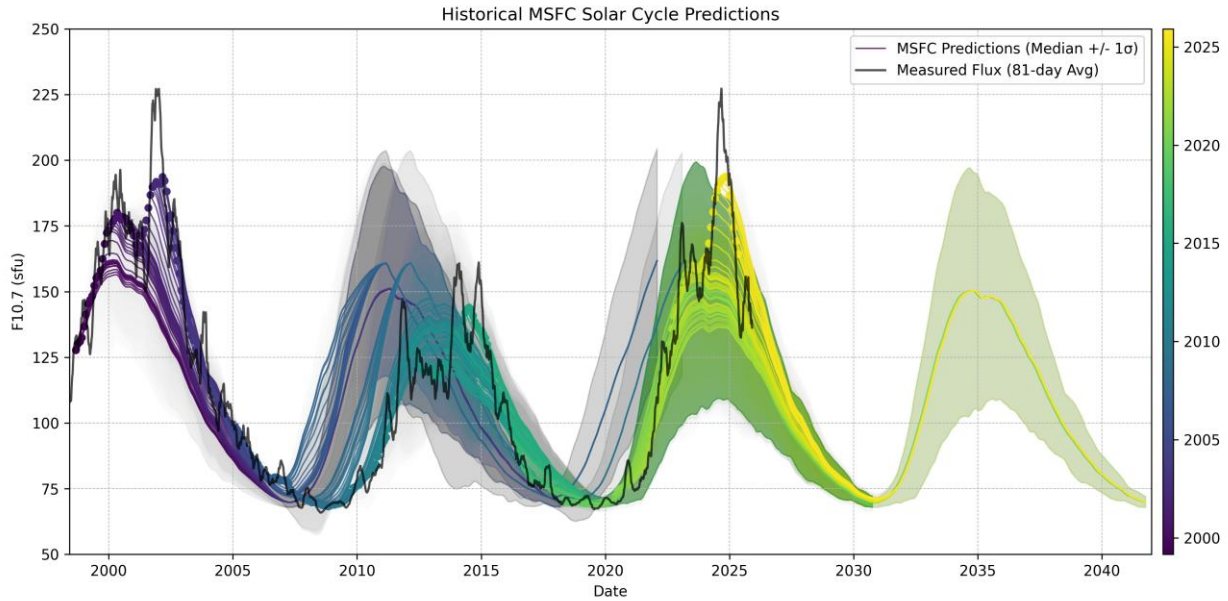


Figure 6: All historical solar cycle predictions from NASA’s MSFC, colored by prediction date and with their ± 1 standard deviation uncertainty range shaded. The measured 81-day average F10.7 solar flux is overlaid in black.

Results

C_B Estimates

The ratio of C_B from the BSTAR drag parameter to the instantaneous C_B for each object skewed low, ranging from 0.03x to 1.3x. This highlights the enormous error incurred when using C_B from BSTAR values for non-SGP4 drag modeling purposes. The shape of the distributions for the instantaneous and filtered C_B values matched well, but the scoring will show the importance of the filtering process on prediction accuracy. Only 2 of the 934 satellites failed to converge on a physically reasonable C_B estimate, giving our filtering process a >99.7% throughput.

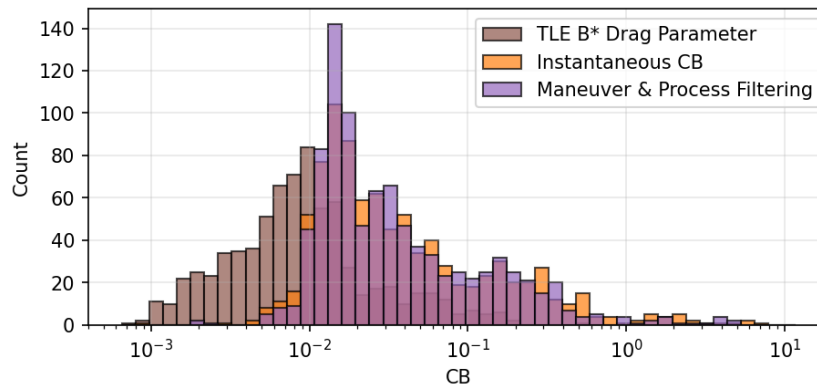


Figure 7: Distribution of C_B estimates for the ensemble of 934 satellites from the three methods of calculating drag from TLEs: BSTAR conversion, instantaneous drag, and filtered drag.

Perfect Knowledge: Known Space Weather and C_B Extracted from Final Year

We start with historical known space weather conditions, and C_B calculated from the final year of data.

Example Propagation

Figure 8 shows a representative example propagation for satellite ID 31134 “OE EDB (INTERSTAGE RING)” with an 8% dispersion. Starting 1 year before the true deorbit date of 2012-09-27, the estimated C_B of $0.031379 \text{ m}^2/\text{kg}$ results in nominally crossing the 300km threshold on 2012-09-14, 4.2 days after the real satellite. The dispersed results have a CRPS of 5.5 days, a median error of +0.3 days, and give the true deorbit date a rank percentile of 0.50. The full range of 20 dispersed cases covers a spread of ± 30 days. These metrics line up almost perfectly with the median ensemble results, so this should help build intuition for what a typical deorbit prediction looks like.

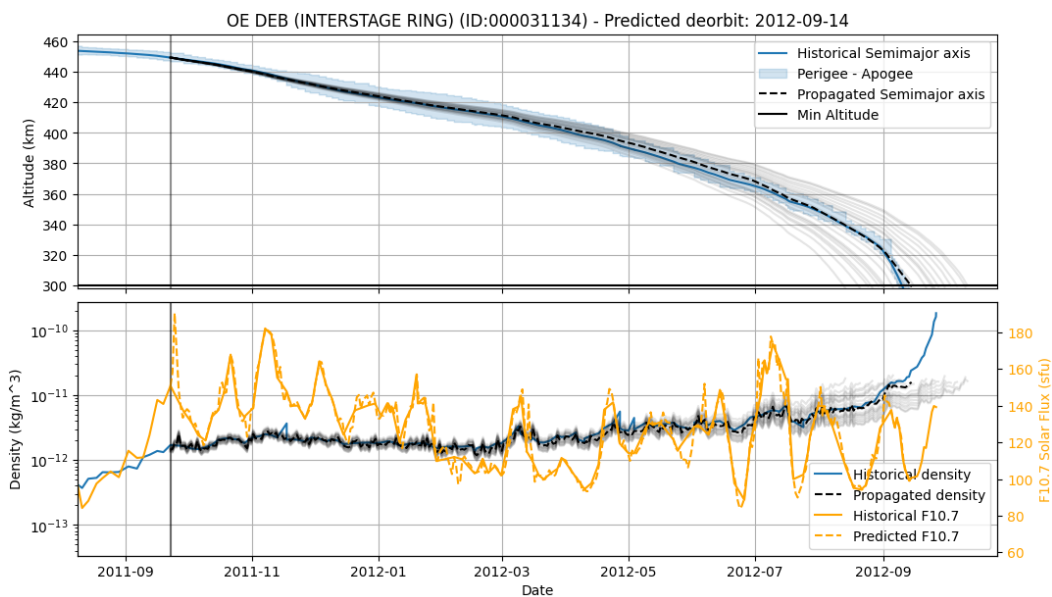


Figure 8: Propagation results for satellite ID 31134. Top plot shows the propagated semimajor axis with the dispersed cases in lighter shading, versus the true historical trajectory. Bottom plot shows the historical F10.7 flux, along with the orbit-average atmospheric density as a result of the satellite altitude and space weather conditions. Note that the predicted F10.7 curve does not perfectly overlay the historical F10.7 because it is sampled at higher frequency than the TLEs.

Dispersion Calibration

Dispersing the simulation improved prediction accuracy. The median CRPS decreased from 8.7 days for a nominal case down to a minimum 5.2 days for a 5% dispersion. The CvM score is minimized for an 8% dispersion, with a 36% improvement relative to a 5% dispersion while only raising the median CRPS to 6.0 days. Because of this small CRPS gap, we choose an 8% dispersion as our baseline estimate of process noise – this gives us the best calibration curve and ensures our distribution of Monte Carlo predictions best matches the true range of outcomes.

A fairly flat median error of 5-6 days extends from the nominal case up through the 15% dispersed case, meaning that on average we overestimate the lifetime of the satellites by this much. We do not apply a bias correction to zero out this expected error and improve the calibration curve, since it is specific to this C_B estimation window.

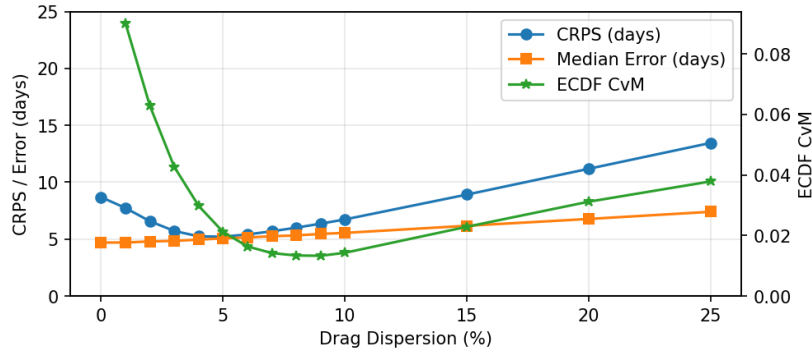


Figure 9: Median ensemble scores as a function of drag dispersion d , for the perfect knowledge scenario (known space weather and C_B from the last year of flight.)

Score Details

Figure 10 shows the distributions of CRPS and median error for the ensemble of satellite deorbit forecasts, as well as the percentile histogram and calibration curves for the 5% and 8% dispersed cases. Each of our processing steps improves predictive power. The C_B values derived from TLE BSTAR terms over-predict the 1-year lifetime by nearly two years. Instantaneous C_B values derived from changes in orbital momentum predict deorbit with a median 45 days of accuracy. Leonid’s maneuver detection and process filtering improves this to 8.7 days. Dispersed predictions at 8% further improve this to 6.0 days, while greatly lowering the portion of predicted ranges which don’t include the true deorbit date at 5% dispersion.

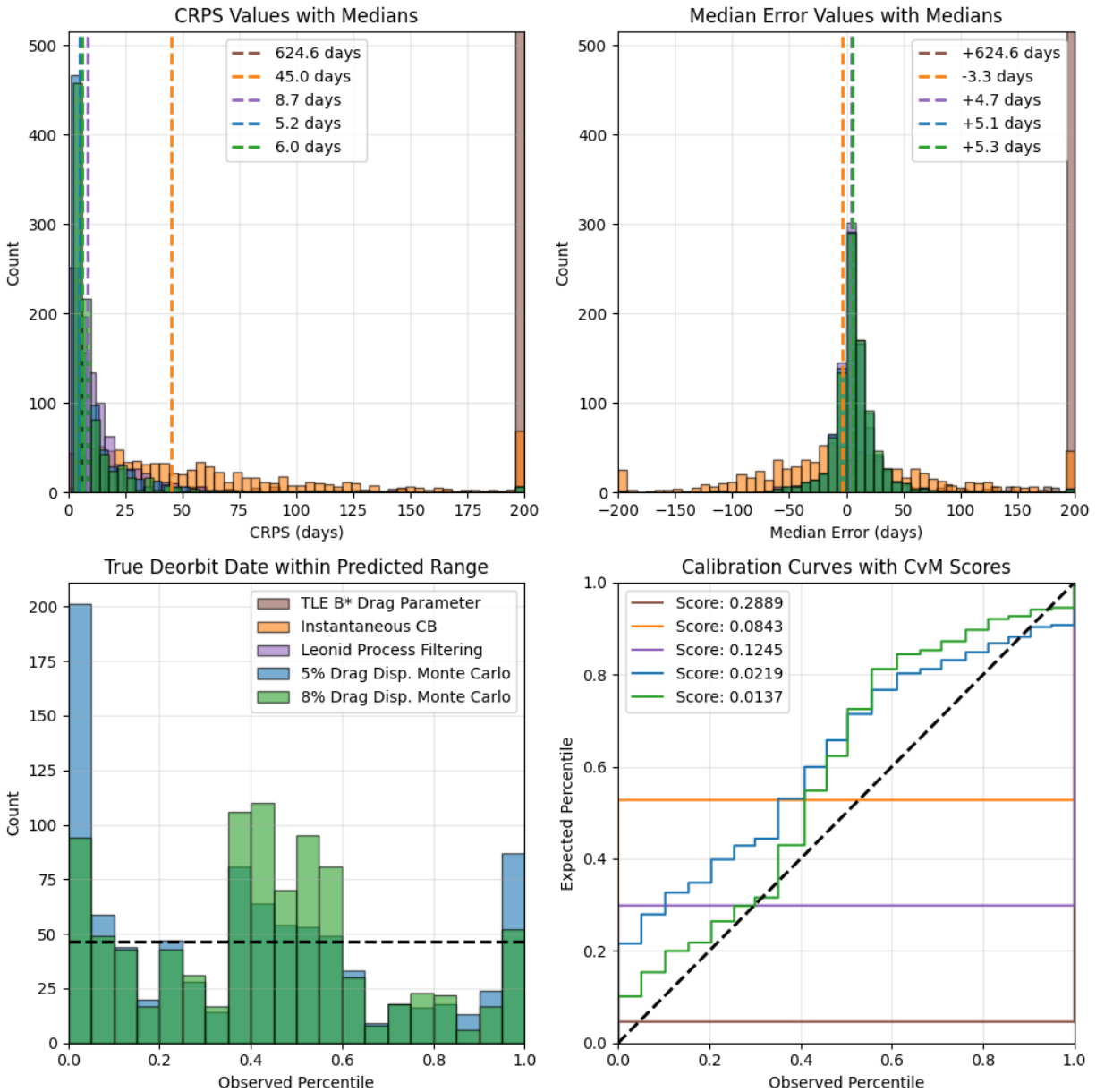


Figure 10: Ensemble prediction results for all 934 satellites for the perfect knowledge scenario (known space weather and C_B extracted from the last year of flight). The top row shows CRPS with the median values marked (top left) and median error with ensemble median values marked (top right). Results greater than 200 days are binned in the rightmost bar. The bottom row shows the percentile ranks of the true deorbit date within the dispersed distributions (bottom left), and the corresponding calibration curves with CvM scores (bottom right).

Estimating C_B from Varying Lookback Windows

For satellites in orbit we only ever have historical data to work with, and must use past ephemerides to estimate C_B . Figure 11 below shows how longer lookback windows improve C_B estimates for a calibrated dispersion, with dispersed CRPS dropping from 26.1 days at a 36% dispersion for a one week lookback to 14.8 days at 19% dispersion for a one year lookback.

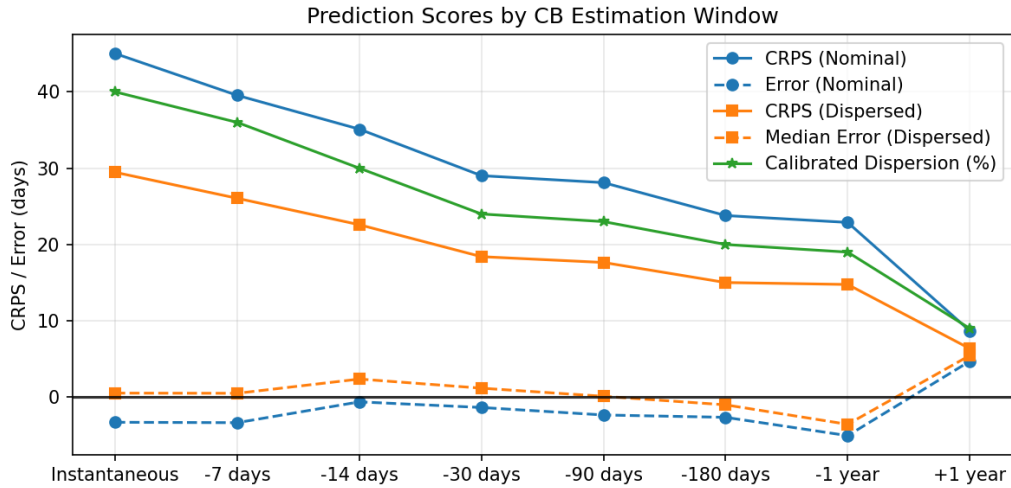


Figure 11: CRPS and median error scores for different C_B calculation lookback windows, showing that predictions improve with more data. The drop in calibrated dispersion percentage demonstrates better filtering of process and measurement noise. Also shows the +1 year period for the “perfect knowledge” scenario.

For this analysis we use a representative 30 day lookback window – this is short enough to be actionable soon after detection of an object on-orbit, and covers one full Carrington rotational period of the Sun which allows for better filtering of the C_B variation happening at that timescale. But for production analyses Leonid uses all available data.

Historical Conditions: Known Space Weather and C_B Estimated from Prior 30 Days

Dispersion Calibration

The median CRPS drops from 29.0 days nominally to a minimum 17.3 days at an 18% dispersion. The CvM score is minimized at a 25% dispersion, where the CRPS is 18.6 days and the median error is +1.2 days.

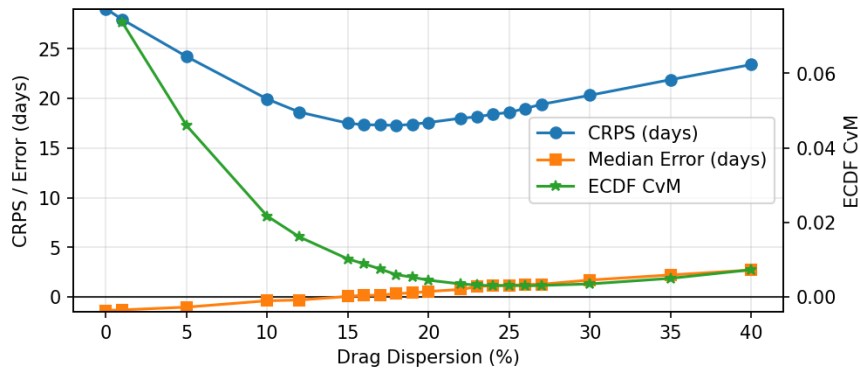


Figure 12: Median ensemble scores as a function of drag dispersion d , for the historical conditions scenario (known space weather and C_B estimated from the prior 30 days).

Score Details

Figure 13 shows the distributions of CRPS and median error for the ensemble of satellite deorbit predictions, as well as the percentile histogram and calibration curves for the 18% and 25% dispersed cases. Each of our processing steps improves predictive power. Leonid’s maneuver detection and process filtering gives 29.0 days of prediction accuracy. Dispersing at $d = 25\%$ improves this to 18.6 days, while greatly lowering the portion of predicted ranges which don’t include the true deorbit date versus the 18% dispersion.

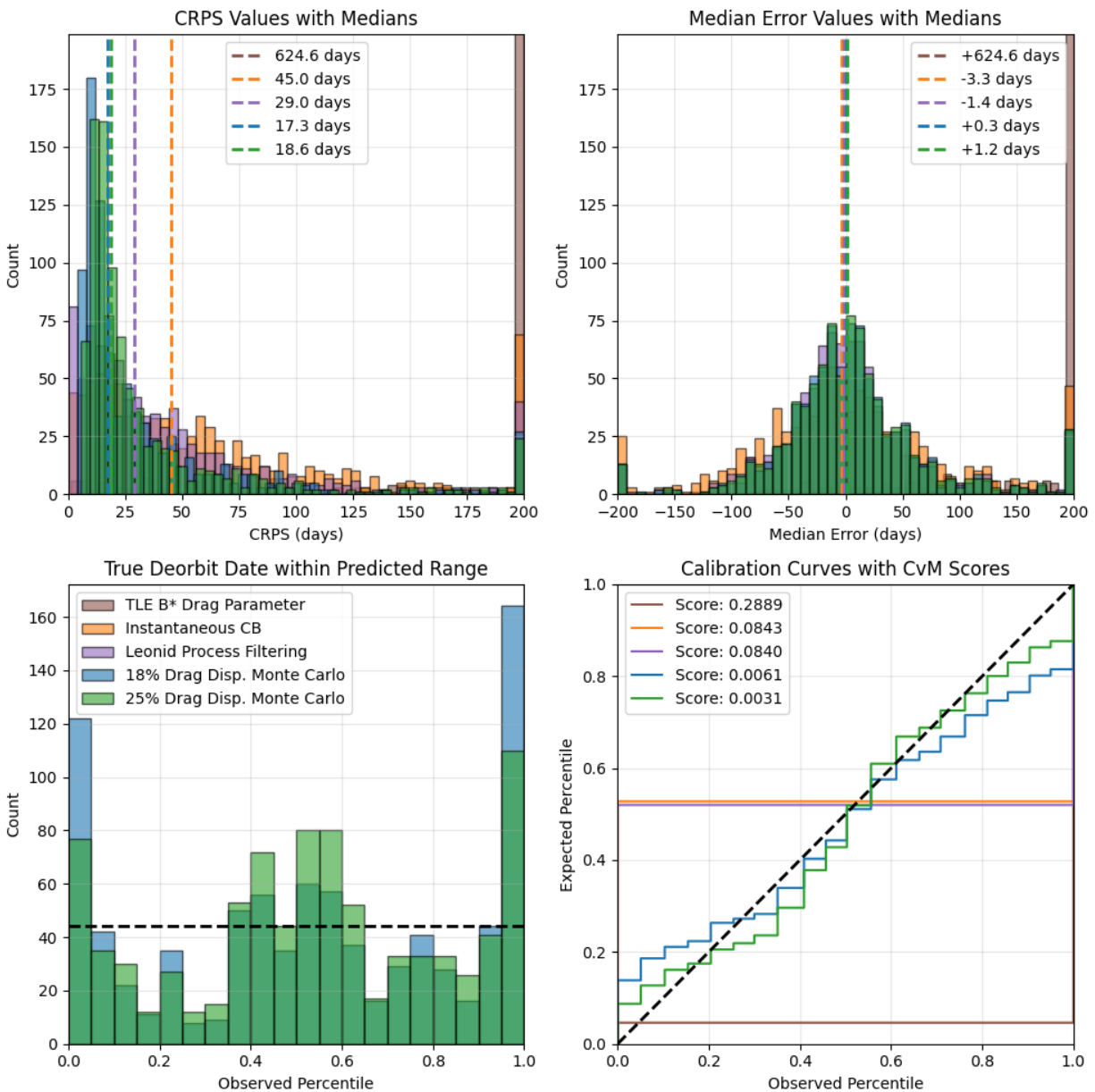


Figure 13: Ensemble prediction results for all 934 satellites for the historical conditions scenario (known space weather and C_B estimated from the prior 30 days of flight data). The top row shows CRPS with the median values marked (top left) and median error with ensemble median values marked (top right). Results greater than 200 days are binned in the rightmost bar. The bottom row shows the percentile ranks of the true deorbit date within the dispersed distributions (bottom left), and the corresponding calibration curves with CvM scores (bottom right).

Fully Predictive: Forecasted Space Weather and C_B Estimated from Prior 30 Days

Since the MSFC solar cycle forecasts only started in March of 1999, we downselect from our test set of 934 satellites to the 415 which reentered after then. In addition to the drag dispersion, we additionally disperse the predicted MSFC flux by a normally-distributed multiple of its standard deviation, and raise the number of dispersed cases to $n = 100$. Of note is that this time period only covers Solar Cycles 23-25, so the errors and CRPS values here are in large part specific to the characteristic deviations of just these three cycles.

Dispersion Calibration

For the fully predictive scenario, the CRPS and CvM scores are essentially flat no matter what the drag dispersion d is set to. Another way to think about this is that over a year, a satellite's trajectory is completely dominated by solar cycle uncertainty. This is consistent with the analysis from [37] and [38] which shows F10.7 flux to be the driving factor in drag sensitivity analysis.

We see a small drop in CRPS from 47.1 days at 0% dispersion to 45.5 at $d = 10\%$, so use that case in the details below. The low CvM here tells us that the uncertainty of MSFC's forecasts is well calibrated as-is, at least on a 1-year time horizon.

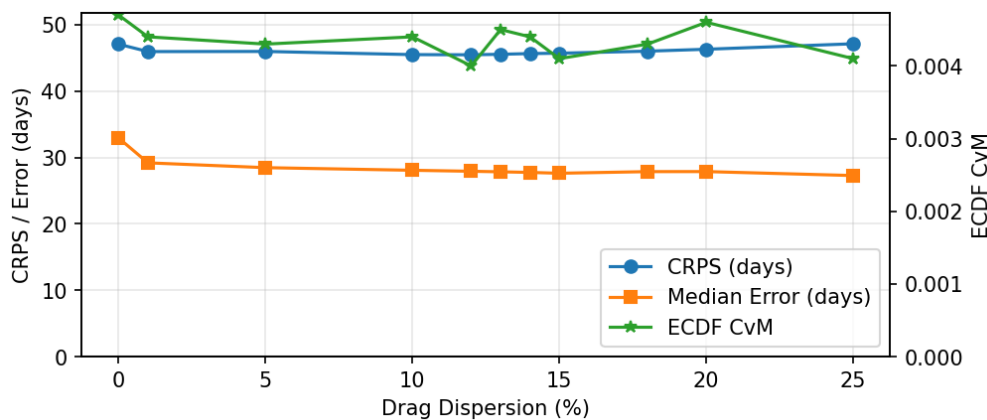


Figure 14: Median ensemble scores as a function of drag dispersion d , for the fully predictive scenario (forecasted space weather and C_B estimated from the prior 30 days). Since the results are flat, the uncertainty is dominated by the solar cycle.

Score Details

Figure 15 shows the distributions of CRPS and median error for the ensemble of satellite deorbit forecasts, as well as the percentile histogram and calibration curve for the fully predictive scenario. With nominally forecasted space weather, the instantaneous C_B gives 78.3 days of accuracy. Leonid's maneuver detection and process filtering drops this down to 67.6 days, and including flux and drag dispersions further improve results to 45.5 days.

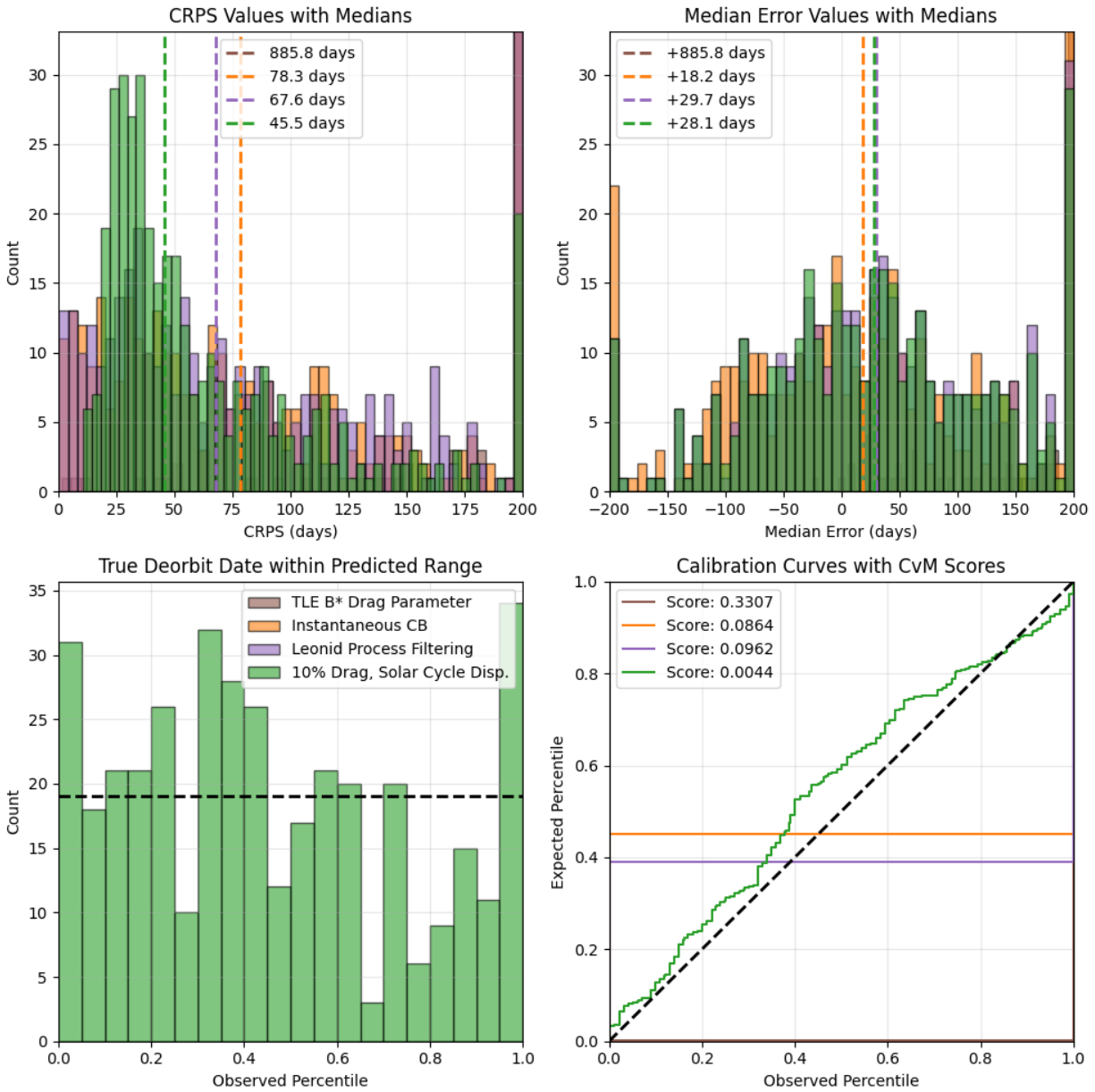


Figure 15: Ensemble prediction results for the 415 satellites since March 1999, for the fully predictive scenario (MSFC forecasted space weather and C_B calculated from the prior 30 days of flight data). The top row shows CRPS with the median values marked (top left) and median error with ensemble median values marked (top right). Results greater than 200 days are binned in the rightmost bar. The bottom row shows the percentile ranks of the true deorbit date within the dispersed distributions (bottom left), and the corresponding calibration curves with CvM scores (bottom right).

Summary of Calibrated Prediction Scores

We collect the CRPS values from each of the validation steps and compare them in Figure 16 below.

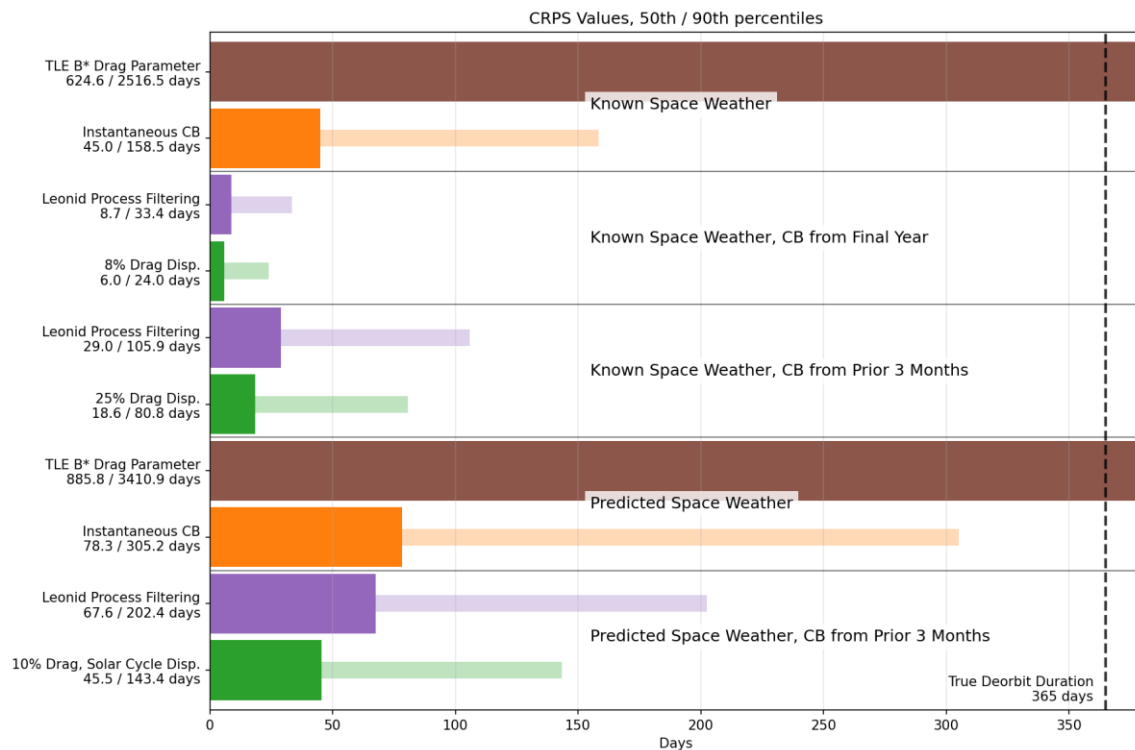


Figure 16: Summary of lifetime prediction CRPS values, showing 50th and 90th percentile scores. Top half of the plot shows accuracy given known space weather conditions, and bottom half uses MSFC solar cycle forecasts.

Comparison against other Lifetime Tools

Leonid can generate reports for US and EU clients which show compliance to their respective satellite lifetime deorbit requirements, using their jurisdictionally designated tools of DAS [39] and DRAMA [40]. French operators also use STELA and OPERA to predict orbital lifetimes [41], but we exclude them from comparison due to low uptake. However, these tools are optimized for ensuring regulatory compliance, and have some architectural limitations for operational use cases:

- No tooling to calculate ballistic coefficients from on-orbit data, defaulting to $C_D = 2.2$.
- DAS has no Monte Carlo analysis ability or ability to disperse solar cycles.
- DRAMA's Monte Carlo ability is limited to its programming interface, and does not extend to space weather. Note that its "Monte Carlo" solar cycle forecast is still a single estimate that samples past cycles, rather than a collection of predictions. Its "Best Case/Worst Case" forecasts can give two point estimates for a given confidence interval, but not a full ensemble [42] [43].
- No tracking of past & projected propellant consumption to offset drag.

This precludes using these tools for real-time on-orbit tracking & future projections, as well as for some of Leonid's standard mission design analyses such as propulsion system sizing, launch date / solar cycle phasing sensitivity, and full dispersed Monte Carlo analysis.

ESA’s Public Tooling: DRAMA & DISCOS

ESA’s Debris Risk Assessment and Mitigation Analysis (DRAMA) software is the primary tool for European Union operators to show compliance with ESA’s Space Debris Mitigation Requirements [44] [45]. We use the Orbital Spacecraft Active Removal (OSCAR) module in DRAMA v4.1.1, which has a Python interface that allows for programmatic analysis [46]. DRAMA provides tooling for estimating frontal area from object shape, but does not provide tooling to estimate C_B from on-orbit data.

So for publicly accessible C_B estimates we turn to ESA’s DISCOS, a database of space objects that lists estimated mass and average cross-sectional area when possible [47] [48]². We downselect our test set of 934 satellites to the 591 in DISCOS which have that area and mass information (see Table 1), and use their recommended $C_D=2.2$ to calculate C_B . Because DRAMA also uses NRLMSISE-00, we can use Leonid’s ballistic coefficient estimates without atmosphere model bias correction. We choose the “historical conditions” scenario with known space weather and Leonid’s C_B from the prior 30 days, since the tool has limited ability to disperse solar cycle futures. Figure 17 shows a representative comparison.

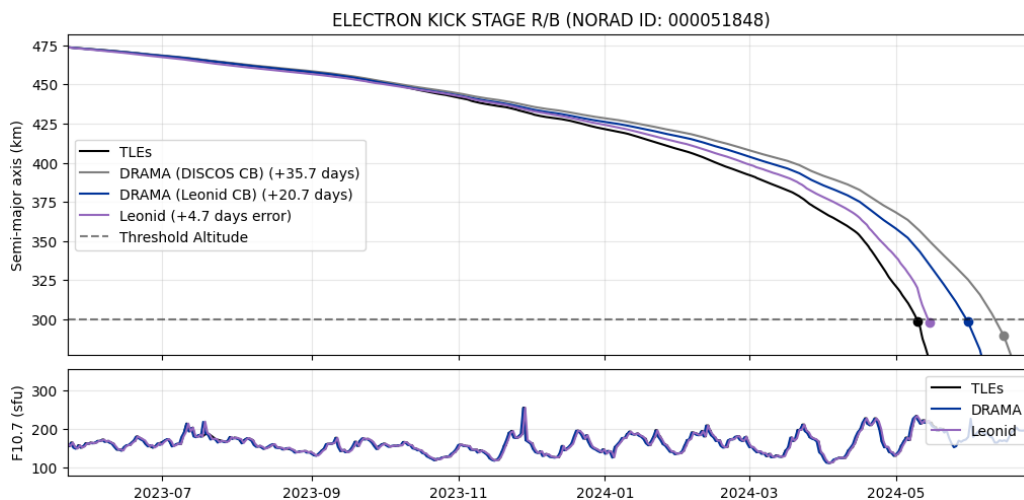


Figure 17: Representative lifetime predictions for NORAD ID 51848 with DRAMA using C_B from DISCOS and from Leonid’s estimates, compared to Leonid’s propagation and ground-truth TLEs. Uses known space weather.

DRAMA has a higher fidelity force model than Leonid’s propagator, and includes the HWM07 wind model, Earth gravitational harmonics above J_2 , SRP, and third body Sun & Moon gravity. However in Figure 18 we see that this extra fidelity does not improve deorbit estimates. First, it’s necessary to estimate C_B – DRAMA’s accuracy improves from 43.0 days to 23.6 days when we switch from DISCOS area- and mass-based estimates to Leonid’s orbit-based ones. Then using Leonid’s propagator improves median prediction accuracy to 10.8 days – a 4x improvement over DRAMA with DISCOS data, and with considerably tighter tails. We measure our propagation as 55x faster than DRAMA, which we attribute primarily to the lower order force model (both are faster than the Orekit DSST reference).

DRAMA has been backtested three times before against reference sets of deorbited satellites. [49] examined 207 rocket bodies in LEO, [30] examined 320, and [50] examined 299 rocket bodies and small satellites. All used C_B calculated from DISCOS data. Extracting the digitized values from Figure 3 in [49]

² For conducting this comparative analysis, we are using information from ESA DISCOS (Database and Information System Characterising Objects in Space), a single-source reference for launch information, object registration details, launch vehicle descriptions, as well as spacecraft information for all trackable, unclassified objects. We acknowledge ESA’s efforts to maintain and operate this database with its APIs.

and both cases from Figure 2(a) in [30], we find all have a median absolute error (equivalent to CRPS for non-dispersed analysis) of 15%, or 54.8 days over a year. Extracting the digitized values from Figures 4 and 5 in [50] we find a median absolute error of 16.6% (60.5 days over a year). These line up well against our test set of 591 objects with a median error of 11.8% (43.0 days).

Note that these are all over a subset of 591 satellites that are well characterized enough to have mass and area estimates. This includes all 392 rocket bodies from the full set, 105 debris, and 94 unknown objects. In some sense, these are more “well behaved” and have less process and measurement noise than the others in the full set. When we use the Leonid C_B and the full set of 934 satellites, the nominal runs for the two match closely and Leonid’s propagator only slightly improves on DRAMA’s (29.0 vs 31.3 days). Dispersing further improves our accuracy to 18.6 days as previously covered.

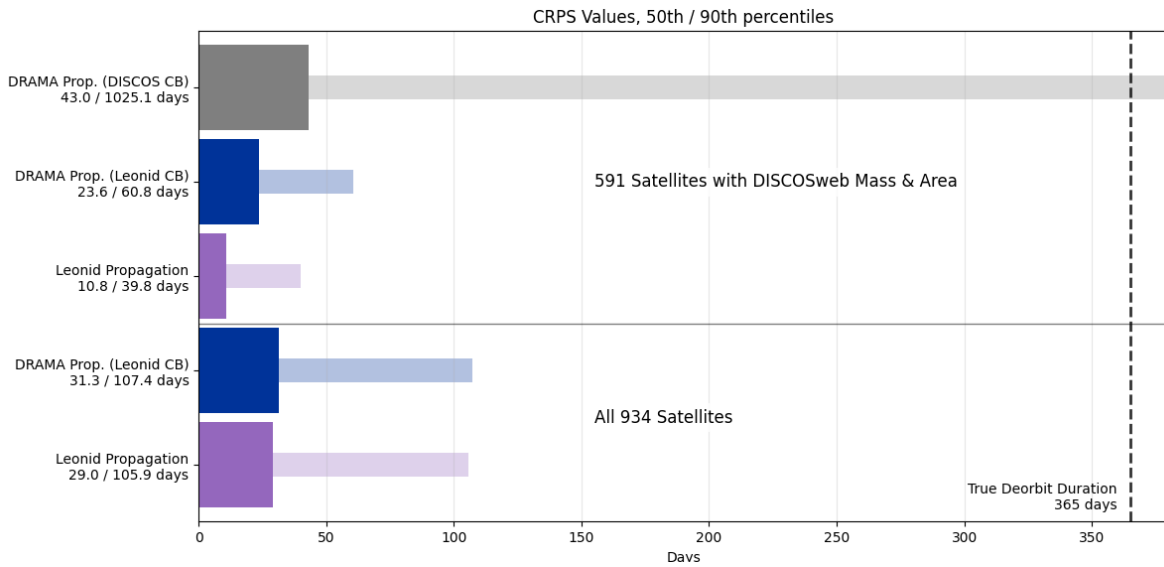


Figure 18: Comparison of absolute error (CRPS) values between Leonid’s and DRAMA’s deorbit predictions, for the 591 satellites with DISCOS mass and area estimates (top), and all 934 satellites (bottom). These are nominal predictions with known space weather, and the Leonid C_B is estimated from the 30 days of prior flight data.

Table 1 shows a breakdown of how many of the objects in the SATCAT have mass & area or decay date estimates available in DISCOS. From their 96% coverage in DISCOS, we expect payloads and rocket bodies to reflect our higher accuracy “well behaved” satellite predictions. We provide C_B coverage over the full set of debris objects, of which only 1.3% currently have existing mass and area estimates.

Category	Total	Mass & Area in DISCOS	% of Total	Pred. Decay in DISCOS	% of Total	Either in DISCOS	% of Total
All LEO	58,823	28,339	48.2%	16,576	28.2%	35,817	60.9%
On-orbit LEO	25,543	14,943	58.5%	16,353	64.0%	22,339	87.5%
On-orbit LEO Payloads	14,041	13,413	95.5%	8,087	57.6%	13,430	95.6%
On-orbit LEO Rocket Bodies	960	919	95.7%	444	46.2%	935	97.4%
On-orbit Debris	9,995	128	1.3%	7,470	74.7%	7,483	74.9%
On-orbit Unknown	547	483	88.3%	352	64.4%	491	89.8%
On-orbit Other	0	0	0%	0	0%	0	0%

Table 1: Breakdown of how many of the 66,420 SATCAT objects have mass and area or predicted deorbit date information in DISCOS, by object type in LEO (apogee < 2000km). Data was pulled 2025-12-05.

ESA’s Internal Tooling

ESA provides point estimates for the deorbit date of 64% of on-orbit SATCAT objects in LEO through DISCOS. Since 1999 these have been generated through a tool called LASCO (Lifetime Assessment of Catalogued Objects), which estimates ballistic coefficients from daily TLEs via a shooting method in its BaPIT (Ballistic Parameter Iteration Tool) module and then propagates through to deorbit via its SOLAT (Simple Orbital Lifetime Assessment Tool) module with SOLMAG space weather forecasts [51] [52] [53] [54]. These are updated in real time without historical data available, so a one-to-one backtest cannot be performed.

A comprehensive backtest of 602 payloads & rocket bodies and 2344 space debris objects was recently performed in [55] using this tooling, following similar methodology as [56]. They report out the results of a “historical conditions” scenario using known space weather and estimated ballistic coefficients. We examine their ensemble results for payloads and rocket bodies, which have much lower errors than their ensemble results for space debris. After digitizing the results in their Figure 12(b) and accounting for the 17% of cases which have >100% prediction error not shown on the plot, we find a median absolute error of 25% (91.3 days over 1 year), with a 90th percentile absolute error of >100% (>365 days). This is less accurate than the DISCOS mass & area approach above, so we defer to that as the state-of-the-art. [55] also performed a “fully predictive” backtesting scenario to compare two nominal solar cycle forecasting methods, but unfortunately the absolute error results are not presented in the paper.

Recently ESA has also developed the Radiation and Atmospheric Drag Coefficient Estimation Routine (RACER) tool to estimate C_B from TLE data [30], however neither RACER nor its outputs are publicly available and cannot be compared here.

NASA’s DAS

NASA’s Debris Analysis Software (DAS) is the de-facto standard lifetime estimation tool used in the United States, as it is the preferred tool to show compliance with the FCC’s 5-year post-mission deorbit rule [57] [58]. We use the python interface introduced in DAS v3.2.7 to enable performing this large-scale comparative analysis. See also [59] for an investigation of DAS’s accuracy.

Since DAS cannot estimate drag parameters from orbit data, we can only benchmark it with C_B from other sources. Note that NASA has no public tooling which estimates ballistic coefficients from publicly available orbit data. Tools like Orekit or TUDAT can perform C_B estimation, however their least-squares and Kalman filter approaches are only suitable to run over a few days of data before solutions start to diverge. A robust approach to find C_B over longer time periods requires a custom piecewise approach followed by maneuver detection and filtering, much like we perform in our processing pipeline. DAS takes in a user-provided area-to-mass ratio and combines with an assumed $C_D = 2.2$, and since DISCOS’s estimates are generated via the same method they provide realistic expected values for someone using the tool. We ran with C_B from both DISCOS and Leonid’s estimator, and divided by DAS’s assumed $C_D = 2.2$ to get the area-to-mass ratio value for its input.

DAS’s PROP3D propagator used for LEO orbits has a higher fidelity force model than Leonid’s propagator, and includes Earth gravitational harmonics above J_2 , SRP, and third body Sun & Moon gravity [60], albeit with the older Jacchia 1977 atmosphere model [61]. In Figure 19 we see that here too this extra fidelity does not improve deorbit estimates. When using Leonid’s C_B estimates we see DAS performance on par

with DRAMA, at a median CRPS of 28.1 days for the DISCOS subset, and 35.1 days for the full set of satellites. However when we use only publicly available C_B estimates from DISCOS then this score jumps to 90.0 days – 8x worse than Leonid’s score of 10.8 days on this subset and with considerably tighter tails. We also measure Leonid’s propagator as 9x faster.

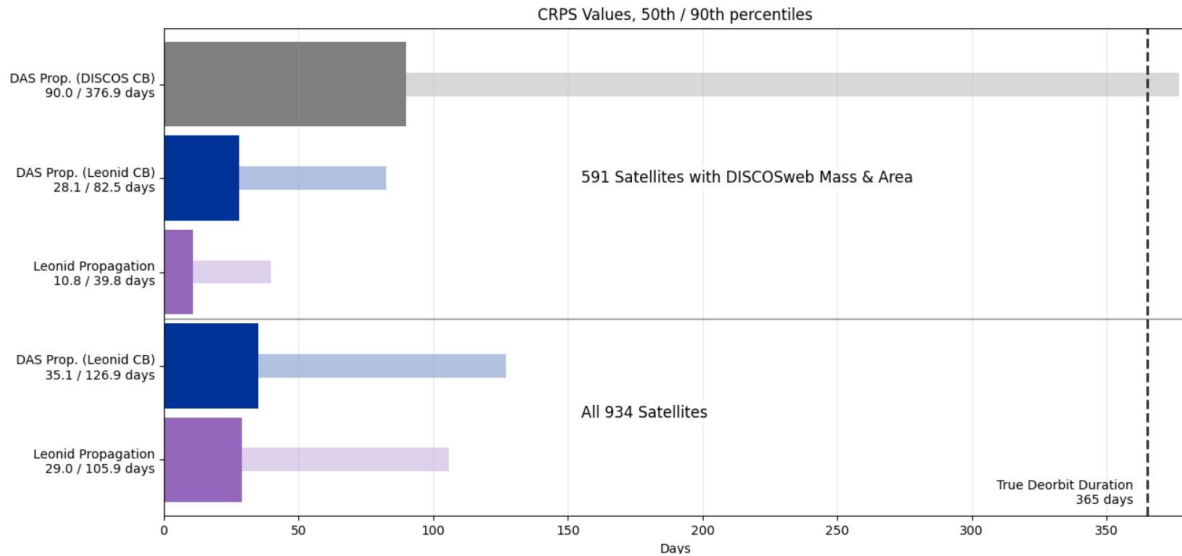


Figure 19: Comparison of absolute error (CRPS) values between Leonid’s and DAS’s deorbit predictions, for the 591 satellites with DISCOS mass and area estimates (top), and all 934 satellites (bottom). These are nominal predictions with known space weather, and the Leonid C_B is estimated from the 30 days of prior flight data.

Conclusion

This report validates Leonid Space's satellite lifetime prediction pipeline against 934 deorbited satellites spanning six decades of spaceflight. Our three-stage validation methodology progressively removed hindsight to quantify accuracy under realistic fully predictive operational conditions. The top-line results are summarized below in Table 2.

Scenario	Space Weather	Ballistic Coefficient	1-Year Accuracy
Perfect Knowledge	Known	Extracted	6.0 days (1.6%)
Historical Conditions	Known	Estimated	18.6 days (5.1%)
Fully Predictive	Forecasted	Estimated	45.5 days (12.4%)

Table 2: Top-line prediction accuracy (median CRPS) results for the three validation scenarios. The percentages show the accuracy relative to the 365-day true remaining lifetime.

The results demonstrate that accurate drag estimation is the critical enabler for lifetime prediction. BSTAR-derived ballistic coefficients are shown to be wholly unsuitable, and our approach of using ballistic coefficients derived from on-orbit data rather than catalog-based mass and area estimates yields a 4x improvement in prediction accuracy over ESA's DRAMA tool with DISCOS data and an 8x improvement over NASA’s DAS. Once ballistic coefficients are properly characterized, solar cycle uncertainty becomes the dominant error source – our analysis shows that varying drag dispersion has negligible effect on prediction accuracy when space weather is forecasted rather than known.

These findings have two implications. First, it validates Leonid's focus on robust ballistic coefficient estimation from TLE data, which extends accurate lifetime prediction to the >98% of tracked on-orbit debris objects lacking mass and area estimates in existing databases. Second, it establishes a new framework for scoring solar cycle forecasts, by grounding forecast accuracy in operationally-relevant satellite lifetime predictions. This lays the groundwork for future development of internal solar cycle forecasting capabilities.

Our propagator's 340x speed advantage over a reference Orekit implementation enables Monte Carlo analysis at scale, turning point estimates into calibrated probability distributions. The validation campaign itself – an ensemble of over 900 satellites, simulated for a number of dispersed cases, across a range of dispersion levels, and repeated for several scenarios – demonstrates this capability.

To our knowledge, this is the first comprehensive backtesting of long-term satellite lifetime predictions that reports quantitative results for the fully predictive case. We qualify this by requiring comparison to real orbit data, setting a modest threshold of “comprehensive” as $n > 100$ satellites, and defining “long duration” prediction as >30 days. This screens out a large number of studies which parametrically evaluate models, focus on small cohorts of selected satellites, or look at short duration conjunction assessments or reentry location predictions. Notable examples in this camp include [14], [36], [41], [52], [62], [63], [64], [65], [66], [67], and [68]. The studies in [21], [30], [49], [50], [51], and [55] all report hindtesting results that fit the qualifying criteria, but only for known historical space weather conditions. [55] looks at a fully predictive scenario, but unfortunately only reports which of two space weather forecasts gives relatively better results rather than quantitative accuracy. The means that these results for Leonid's analysis pipeline are uniquely valuable in an operational context where the future is not yet known.

The results here are based on TLE data and non-payload objects that are tumbling without attitude control. This is a harder test set than stable payload platforms. When working with payload operators, Leonid's analysis can use higher-fidelity onboard GPS telemetry and include orbit control plans, propulsion system characteristics, and attitude control schemes. Using this higher fidelity data will eliminate process and measurement noise sources – for those clients we expect that our prediction accuracy will only improve on the results here.

Leonid Space is ready to support LEO satellite operators, regulators, and space domain awareness partners with quantified risk assessments and actionable lifetime predictions. Future work will extend this validation to maneuvering payloads and quantify prediction accuracy across different time horizons.

References

- [1] W. S. Shambaugh, "Doing battle with the sun: lessons from LEO and operating a satellite constellation in the elevated atmospheric drag environment of Solar Cycle 25," in *Small Satellites Systems and Services Symposium (4S 2024)*, 2025.
- [2] SpaceX, "Geomagnetic Storm and Recently Deployed Starlink Satellites," 8 February 2022. [Online]. Available: <https://www.spacex.com/updates>.
- [3] C. Yap, M. Siegers, A. M. L. Valle, R. t. Nallapu, I. Demir, K. Devaraj and S. McIntosh, "Operational Responses to LEO Satellite Orbital Decay during the 25th Solar Cycle Maximum," in *Advanced Maui Optical and Space Surveillance Technologies Conference (AMOS)*, 2024.
- [4] X. Wang, R. Wang, K. Wang, Z. Yang, T. Ren, J. Cao, M. Li, S. Liu, B. Luo and C. Wang, "Premature Reentry of the Binar CubeSats Due To Underestimation of Solar and Geomagnetic Activities and Its Implication for Importance of Medium- and Long-Term Space Weather Forecasts," *Space Weather: The International Journal of Research and Applications*, 30 11 2025.
- [5] Leonid Space, "NASA TROPICS Sample Deorbit Report," 2025.
- [6] D. G. King-Hele, "The contraction of satellite orbits under the influence of air drag, III. High-eccentricity orbits ($0.2 \leq e < 1$)," *Proceedings of the Royal Society of London. Series A. Mathematical and Physical Sciences*, vol. 267, no. 1331, pp. 541-557, 1962.
- [7] V. Martinusi, L. Dell'Elce and G. Kerschen, "Analytic propagation of near-circular satellite orbits in the atmosphere of an oblate planet," *Celestial Mechanics and Dynamical Astronomy*, vol. 123, no. 1, pp. 85-103, 2015.
- [8] S. Frey, C. Colombo and S. Lemmens, "Extension of the King-Hele orbit contraction method for accurate, semi-analytical propagation of non-circular orbits," *Advances in Space Research*, vol. 64, no. 1, pp. 1-17, 2019.
- [9] J. He, "Comparison of empirical and theoretical models of the thermospheric density enhancement during the 3–4 February 2022 geomagnetic storm," *Space Weather*, vol. 21, no. 9, p. e2023SW003521, 2023.
- [10] S. Mutschler, "A Survey of Current Operations-Ready Thermospheric Density Models for Drag Modeling in LEO Operations," in *Advanced Maui Optical and Space Surveillance Technologies Conference (AMOS)*, 2023.
- [11] P. Mesalles-Ripoll, R. Rositani and M. Duncan, "Low-Earth orbit prediction accuracy review of modern empirical atmospheric models and space weather data sources," in *Advanced Maui Optical and Space Surveillance Technologies Conference*, 2023.

- [12] P. Mesalles-Ripoll, "Beyond Density Alone: Accuracy Assessment of Atmospheric Models for Orbit Prediction from a Satellite Operator's Perspective," in *Advanced Maui Optical and Space Surveillance Technologies Conference (AMOS)*, 2025.
- [13] E. Stevenson, B. Bastida Virgili, S. Lemmens and B. Reihs, "Comparison of Atmosphere Models for Low-Altitude Re-entry Predictions," in *4th International Space Debris Re-entry Workshop (ISDRW04)*, 2018.
- [14] B. Bastida Virgili, S. Lemmens and E. Stevenson, "The Impact of the New NRLMSIS 2.0 on Re-Entry Predictions," in *8th European Conference on Space Debris (SDC-8)*, 2021.
- [15] G. Lucas, "pymssis (v0.11.0)," Zenodo, 2025.
- [16] J. Picone, "NRLMSISE-00 empirical model of the atmosphere: Statistical comparisons and scientific issues," *Journal of Geophysical Research: Space Physics*, vol. 107, no. A12, pp. SIA-15, 2002.
- [17] W. S. Shambaugh, "Monaco: A Monte Carlo Library for Performing Uncertainty and Sensitivity Analyses," in *SciPy*, 2022.
- [18] . maisonobe, "CS-SI/Orekit: 13.1.2," Zenodo, 2025.
- [19] P. J. Cefola, "Revisiting the DSST standalone orbit propagator," *Advances in the Astronautical Sciences*, vol. 152, pp. 2891-2914, 2014.
- [20] D. Vallado, "Revisiting spacetrack report #3," in *AIAA/AAS astrodynamics specialist conference and exhibit*, 2006.
- [21] D. J. Gondelach, "Orbit Prediction and Analysis for Space Situational Awareness," University of Surrey, 2020.
- [22] B. Rhodes, "Skyfield: Generate high precision research-grade positions for stars, planets, moons, and Earth satellites," *Astrophysics Source Code Library*, 2019.
- [23] E. Ergene, "Ballistic Coefficient Estimation Methods Using Two-Line Elements," Politecnico di Milano, 2023.
- [24] C. L. Hassa, D. B. Spencer and S. G. Bilén, "Drag coefficient estimation using satellite attitude and orbit data," *Advances in the Astronautical Sciences*, vol. 152, pp. 1985-2002, 2014.
- [25] J. Sang, J. C. Bennett and C. H. Smith, "Estimation of ballistic coefficients of low altitude debris objects from historical two line elements," *Advances in Space Research*, vol. 51, no. 10, pp. 2029-2038, 2013.
- [26] D. J. Gondelach, R. Armellin and A. A. Lidtke, "Ballistic Coefficient Estimation for Reentry Prediction of Rocket Bodies in Eccentric Orbits Based on TLE Data," *Mathematical Problems in Engineering*, vol. 2017, pp. Article ID 7309637, 13 pages, 2017.

- [27] A. Saunders, G. G. Swinerd and H. G. Lewis, "Deriving Accurate Satellite Ballistic Coefficients from Two-Line Element Data," *Journal of Spacecraft and Rockets*, vol. 49, no. 1, pp. 175-184, 2012.
- [28] T. S. Kelso, "Celestrak Satellite Catalog," 2025. [Online]. Available: <https://celestrak.org>.
- [29] United States Space Command, 18th SDS, "space-track.org," 2025. [Online]. Available: <https://www.space-track.org/>.
- [30] L. Ayala Fernández, C. Wiedemann, S. Silvestri, V. Braun and S. Lemmens, "Post-Mission Disposal Considerations for Rocket Stages," in *9th European Conference on Space Debris (SDC-9)*, 2025.
- [31] J. Matzka, "The geomagnetic Kp index and derived indices of geomagnetic activity," *Space Weather*, vol. 19, no. 5, 2021.
- [32] K. O. Niehuss, H. C. Euler Jr. and W. W. Vaughan, "Statistical Technique for Intermediate and Long-Range Estimation of 13-Month Smoothed Solar Flux and Geomagnetic Index," NASA, 1996.
- [33] R. J. Suggs, "Future Solar Activity Estimates for Use in Prediction of Space Environmental Effects on Spacecraft Orbital Lifetime and Performance," National Aeronautics and Space Administration, George C. Marshall Space Flight Center, Huntsville, 2016.
- [34] A. G. McNish and J. V. Lincoln, "Prediction of Sunspot Numbers," *Eos, Transactions American Geophysical Union*, vol. 30, no. 5, pp. 673-685, 1949.
- [35] M. S. Miesch, "Solar cycle prediction at NOAA's space weather prediction center," *Space Weather*, vol. 23, no. 6, p. e2025SW004444, 2025.
- [36] B. J. Naász, K. Berry and K. Schatten, "Orbit Decay Prediction Sensitivity to Solar Flux Variations," in *AAS/AIAA Astrodynamics Specialist Conference*, 2007.
- [37] L. Dell'Elce and G. Kerschen, "Probabilistic Assessment of Lifetime of Low-Earth-Orbit Spacecraft: Uncertainty Propagation and Sensitivity Analysis," *Journal of Guidance, Control, and Dynamics*, vol. 38, no. 5, pp. 886-899, 2015.
- [38] L. Dell'Elce, M. Arnst and G. Kerschen, "Probabilistic Assessment of the Lifetime of Low-Earth-Orbit Spacecraft: Uncertainty Characterization," *Journal of Guidance, Control, and Dynamics*, vol. 38, no. 5, pp. 900-912, 2015.
- [39] NASA Orbital Debris Program Office, *Debris Assessment Software v3.2.7*, 2025.
- [40] ESA, *DRAMA 4.1.1 (pyDRAMA)*, ESA Space Debris Office, 2025.
- [41] C. Le Fèvre, H. Fraysse, V. Morand, A. Lamy, C. Cazaux, P. Mercier, C. Dental, F. Deleflie and D. Handschuh, "Compliance of disposal orbits with the French Space Operations Act: the Good Practices and the STELA tool," *Acta Astronautica*, vol. 94, no. 1, pp. 234-245, 2014.
- [42] V. Braun, N. Sánchez-Ortiz, J. Gelhaus, C. Keschull, S. K. Flegel, M. Möckel, C. Wiedemann, H. Krag and P. Vörsmann, "Upgrade of the ESA DRAMA OSCAR Tool: Analysis of Disposal Strategies

- Considering Current Standards for Future Solar and Geomagnetic Activity," in *6th European Conference on Space Debris (SDC-6)*, 2013.
- [43] V. Braun, S. K. Flegel, J. Gelhaus, C. Keschull, M. Möckel, J. Radtke, C. Wiedemann, H. Krag and P. Vörsmann, "Impact of Solar Flux Modeling on Satellite Lifetime Predictions," in *International Astronautical Congress (IAC) / Space Debris Symposium*, 2012.
- [44] ESA, "ESA Space Debris Mitigation Compliance Verification Guidelines – ESSB-HB-U-002, Issue 3," European Space Agency, 2025.
- [45] ESA, "ESA Space Debris Mitigation Requirements – ESSB-ST-U-007, Issue 1," European Space Agency, 2023.
- [46] V. Braun, J. Gelhaus, C. Keschull, S. K. Flegel, M. Möckel, J. Radtke, C. Wiedemann, H. Krag and P. Vörsmann, "Orbital Lifetime Estimation using ESA's OSCAR tool," in *5th European Conference for Aerospace Sciences (EUCASS)*, München, 2013.
- [47] H. Klinkrad, "DISCOS – ESA's Database and Information System Characterising Objects in Space," *Advances in Space Research*, vol. 11, no. 12, pp. 43-52, 1991.
- [48] ESA, "Database and Information System Characterising Objects in Space (DISCOS)".
- [49] V. Braun, S. Lemmens, H. Krag, T. Flohrer, K. Merz, B. Bastida Virgili and Q. Funke, "Probabilistic Orbit Lifetime Assessment with OSCAR," in *6th International Conference on Astrodynamics Tools and Techniques (ICATT)*, 2016.
- [50] A. Operti, V. Braun, S. Lemmens and S. Corpino, "Assessing Uncertainties in the Estimation of the Orbital Lifetime," in *7th European Conference on Space Debris (SDC-7)*, 2017.
- [51] K. D. Bunte, H. Sdunnus, J. C. Mandeville and H. Klinkrad, "Ballistic parameter and lifetime assessment for catalogued objects," in *3rd European Conference on Space Debris (ESOC, Darmstadt)*, 2001.
- [52] S. Lemmens, B. Bastida Virgili, V. Braun, T. Flohrer, Q. Funke, H. Krag, F. McLean and K. Merz, "From End-of-Life to Impact on Ground: An Overview of ESA's Tools and Techniques to Predict Re-entries from the Operational Orbit Down to the Earth's Surface," in *6th International Conference on Astrodynamics Tools and Techniques (ICATT)*, 2016.
- [53] R. Mugellesi-Dow, D. J. Kerridge, T. D. G. Clark and A. W. P. Thompson, "SOLMAG: an operational system for prediction of solar and geomagnetic activity indices," in *1st European Conference on Space Debris (SDC-1)*, 1993.
- [54] T. Flohrer, S. Lemmens, B. Bastida Virgili, H. Krag, H. Klinkrad, E. Parrilla, N. Sanchez, J. Oliveira and F. Pina, "DISCOS – Current Status and Future Developments," in *6th European Conference on Space Debris (SDC-6)*, 2013.

- [55] E. Petrova, T. Podladchikova, A. M. Veronig, S. Lemmens, B. Bastida Virgili and T. Flohrer, "Medium-term Predictions of F10.7 and F30 cm Solar Radio Flux with the Adaptive Kalman Filter," *The Astrophysical Journal Supplement Series*, vol. 254, no. 1, p. 9, 2021.
- [56] B. Bastida Virgili, S. Lemmens and T. Flohrer, "Practicalities of Re-entry Predictions – The VEGA-01 AVUM Case," in *7th European Conference on Space Debris (SDC-7)*, 2017.
- [57] United States Federal Communications Commission, *47 CFR §25.114(d)(14)(vii)(D)(1)*, U.S. Government Publishing Office, 2025.
- [58] NASA, "NASA-STD 8719.14 Revision A with Change 1: Process for Limiting Orbital Debris," National Aeronautics and Space Administration, 2012.
- [59] Y. Chandramouli and L. Shockley, "A Sensitivity Analysis of DAS Lifetime Collision Probability Estimates," in *Advanced Maui Optical and Space Surveillance Technologies Conference (AMOS)*, 2025.
- [60] J. C. Liou, "Debris Assessment Software User's Guide NASA/TP-20210025946," 2021.
- [61] L. G. Jacchia, "Thermospheric Temperature, Density and Composition: New Models," Smithsonian Astrophysical Observatory, Special Report 375, 1977.
- [62] E.-J. Choi, S. Cho, D.-J. Lee, S. Kim and J. H. Jo, "A Study on Re-entry Predictions of Uncontrolled Space Objects for Space Situational Awareness," *Journal of Astronomy and Space Sciences*, vol. 34, no. 4, pp. 289-302, 2017.
- [63] D. Oltrogge and D. A. Vallado, "Satellite Lifetime and Solar Cycle Predictions," in *8th European Conference on Space Debris (SDC-8)*, Darmstadt, 2021.
- [64] C. Pardini and L. Anselmo, "Assessing the Risk and the Uncertainty Affecting the Uncontrolled Re-entry of Manmade Space Objects," *Journal of Space Safety Engineering*, vol. 5, no. 1, pp. 46-62, 2018.
- [65] N. Sánchez-Ortiz, N. Guijarro López, I. Grande, L. Tabera, A. White, S. Bruinsma and S. Lemmens, "Re-entry Prediction Uncertainties Derived from Environmental and Observation Considerations," in *7th European Conference on Space Debris*, Darmstadt, 2017.
- [66] C. Pardini and L. Anselmo, "Re-Entry Predictions for Uncontrolled Satellites: Results and Challenges," in *Safety Is Not an Option, Proceedings of the 6th IAASS Conference*, Montreal, 2013.
- [67] E. David and V. Braun, "Re-entry Analysis Comparison with Different Solar Activity Models of Spent Upper Stage Using ESA's DRAMA Tool," in *6th IAASS Conference*, Montreal, 2013.
- [68] W. E. Parker, M. Freeman, G. Chisham, A. Kavanagh, P. M. Siew, V. Rodriguez-Fernandez and R. Linares, "Influences of Space Weather Forecasting Uncertainty on Satellite Conjunction Assessment," *Space Weather*, no. n/a, 2024.

Appendix 1: List of Satellites Used

This is a list of the NORAD IDs for all 934 satellites used in the study. The subset of 591 satellites marked with * have mass and area information available in DISCOS.

23*, 28*, 30*, 64*, 79, 129, 135, 139, 140, 142, 146, 151, 157, 161, 165*, 166, 229*, 257*, 288*, 311*, 313, 388*, 398*, 400, 514, 519*, 534*, 535, 582, 603*, 605*, 606*, 607*, 610, 611, 615, 684, 685, 686, 696*, 697, 699, 717*, 744*, 749*, 760, 761, 775*, 874, 875, 878*, 925, 926, 927, 988*, 1092*, 1098*, 1228*, 1248, 1270*, 1289*, 1336, 1338, 1339, 1340, 1341, 1342, 1343, 1344, 1345, 1346, 1347, 1348, 1351, 1354, 1370, 1371, 1372, 1373, 1376, 1378*, 1397, 1398, 1402, 1448*, 1449, 1461, 1473, 1581, 1640*, 1649, 1650, 1657, 1661, 1664, 1667, 1676, 1677, 1685, 1687, 1690, 1691, 1700, 1709, 1717, 1723, 1725, 1747, 1748, 1750, 1753, 1758, 1761, 1770, 1822*, 1823, 1828, 1830, 1832, 1842*, 1844*, 1852, 1860, 1869*, 1871, 1872, 1873, 1875, 1876, 1877, 1878, 1881, 1885, 1906, 1907, 1919, 1934, 1935, 1936, 1937, 1938, 2098, 2145, 2169*, 2257*, 2519*, 2614, 2681, 2689, 2692, 2696*, 2704*, 2721*, 2763*, 2774*, 2823, 2894*, 2896*, 2897*, 2958, 2987, 3004*, 3011*, 3019*, 3023*, 3102*, 3103, 3146*, 3151*, 3234*, 3283*, 3328, 3349*, 3527*, 3546, 3547*, 3548, 3664*, 3828*, 3836*, 3844, 3849, 3851, 3852, 3853, 3859, 3860, 3861, 3862, 3863, 3865, 3867, 3870, 3879, 3881, 3921, 3933, 3987*, 4120*, 4134, 4153, 4156, 4160, 4165, 4167, 4170, 4172, 4181, 4196, 4203, 4206, 4215, 4260, 4268, 4274*, 4335, 4350*, 4361*, 4498*, 4584*, 4714*, 4802*, 4807*, 4814*, 4827, 4834, 4850*, 4923*, 4927, 4956*, 5041*, 5135*, 5139, 5141, 5143*, 5164, 5254*, 5268, 5278, 5282*, 5311, 5318*, 5320, 5328*, 5330, 5399, 5405, 5462*, 5467*, 5499*, 5602, 5629*, 5644*, 5676*, 5815*, 5818, 5819, 5853*, 5880*, 5895*, 5932, 6098*, 6146, 6156, 6221, 6244, 6273*, 6329*, 6344*, 6345, 6351*, 6352, 6374*, 6634*, 6637*, 6638*, 6641, 6643*, 6651, 6733, 6780, 6781, 6800*, 6803*, 6804, 6908*, 6912*, 6951*, 7004*, 7110*, 7111, 7215, 7302*, 7307*, 7326*, 7338*, 7340*, 7348*, 7418*, 7450, 7470*, 7472*, 7577*, 7581, 7636, 7638*, 7639, 7650*, 7713*, 7753*, 7804, 7806, 7969*, 7971*, 8010*, 8037*, 8044*, 8107, 8128*, 8333*, 8337, 8364*, 8445*, 8472*, 8531*, 8605*, 8689*, 8690, 8745*, 8755*, 8795*, 8814*, 8866*, 8904*, 8931*, 9054*, 9056*, 9390*, 9404*, 9410, 9576*, 9604*, 9605, 9625*, 9802*, 9842*, 9854*, 9884*, 9899*, 10029*, 10069*, 10130*, 10135*, 10179, 10190, 10212, 10223, 10226, 10233, 10236, 10246, 10255, 10267, 10313, 10348, 10363*, 10377*, 10378*, 10431*, 10503*, 10582*, 10819*, 10853, 10854, 10861*, 10899*, 10914*, 11056*, 11083*, 11151*, 11156*, 11162*, 11252*, 11263*, 11269*, 11271*, 11279*, 11280*, 11286*, 11322, 11332*, 11383*, 11393*, 11450*, 11458*, 11601*, 11610*, 11630*, 11683*, 11704*, 11707*, 11742*, 11775, 11776, 11782, 11797*, 11822*, 11830*, 11849*, 11933*, 12017*, 12072*, 12155*, 12163*, 12308*, 12345, 12356, 12357, 12359, 12362, 12389*, 12405, 12626*, 12651, 12689, 12691, 12702, 12721, 12734, 12754, 12761, 12763, 12765, 12846*, 12853*, 12872*, 12969*, 13043*, 13119*, 13368*, 13696*, 13705, 13707, 13708, 13712, 13713, 13716, 13717, 13737, 13738, 13751*, 13774*, 13830*, 13924, 13973*, 14003*, 14004, 14007*, 14076*, 14088*, 14317*, 14381*, 14484*, 14575*, 14609, 14610, 14669*, 14693*, 14694*, 14713*, 14723*, 14724, 14782*, 14824, 14848*, 14927, 14953*, 14970, 15043*, 15067*, 15081*, 15173*, 15242*, 15329*, 15356*, 15363*, 15371, 15409*, 15448*, 15456*, 15499*, 15557, 15569*, 15585*, 15613, 15650*, 15754, 15834*, 15868*, 16014*, 16015*, 16016*, 16017*, 16108*, 16111*, 16121*, 16135*, 16286*, 16330*, 16373*, 16438, 16439*, 16440, 16714*, 16739, 16742*, 16844*, 16865, 16866, 16905, 16929*, 16931*, 16970*, 16983, 16988, 17051*, 17244*, 17327*, 17400, 17402, 17404, 17405, 17407, 17414, 17415, 17481*, 17489, 17492, 17493, 17494, 17495, 17498, 17499, 17502, 17521, 17756, 17786*, 17852, 18014*, 18102*, 18127, 18159, 18191, 18224, 18229, 18238, 18846, 18955, 18984, 19339*, 19764, 20065*, 20303*, 20358*, 20362*, 20390*, 20582*, 20609*, 20639*, 20847, 20851, 20854, 20856, 20857, 20859, 20860, 20869, 20871, 20880, 20882, 20919*, 20960*, 20967*, 21080*, 21150*, 21191*, 21298, 21690*, 21695*, 21825*, 21868*, 21931*, 22013*, 22015*, 22232*, 22298, 22346, 22378, 22401, 22428, 22447*, 22508, 22510, 22522*, 22583*, 22587, 22628, 22658*, 22780*, 22876*, 22878*, 23020*, 23100*, 23277*, 23281, 23502*, 23595, 23677*, 23769*, 23834*, 23854*, 23858*, 23878*, 23941*, 23954*, 24294*, 24323*, 24745*, 24746*, 24777*, 24780*, 24972*, 25014*, 25018*, 25031*, 25124*, 25125*, 25137, 25139, 25176*, 25235*, 25236*, 25310*, 25391*, 25392*, 25393*, 25422*, 25547*, 25647*, 25648, 25694*, 25723*, 25737*, 25738*, 25887*, 25987*, 25988*, 26034*, 26415*, 26482*, 26551*, 26623*, 26632*, 26708, 26874*, 27070, 27075, 27076, 27083, 27084, 27085, 27090, 27093, 27125, 27127, 27131, 27134, 27151, 27412*, 27551*, 27611*, 27644*, 27700*, 27701*, 28099*, 28416*, 28471*, 28506*, 28643*, 28813*, 28942*, 29053*, 29080*, 29093*, 29158*, 29159*, 29253*, 29394*, 29480*, 29508*, 29561, 29654*, 29659*, 30778*, 31134*, 31572, 31700*, 31790*, 31798*, 32284*, 32290*, 32477*, 32751*, 32766*, 33245*, 33317*, 33322*, 33324, 33327, 33329, 33333, 33411*, 33435*, 33457*, 34809*, 34840*, 35006*, 35687*, 36134*, 36607*, 36801, 36835*, 37182*, 37797*, 37942*, 38086*, 38249*, 38864*, 39000*, 39069*, 39229*, 39364*, 39369*, 39409*, 39449*, 39454*, 40048*, 40120*, 40304*, 40306*, 40354*, 40537*, 40913*, 41172*, 41333*, 41395*, 41440, 41441, 41442, 41620*, 41621, 41635*, 41775*, 41902*, 42052*, 42800*, 42902*, 42922*, 42927*, 42993*, 43025*, 43033*, 43101*, 43112, 43116*, 43153*, 43164*, 43173*, 43240, 43520, 43637*, 43658*, 43663*, 43668*, 43669*, 43673*, 43674*, 43739*, 43832*, 43838*, 43840*, 43843*, 43851*, 43853*, 43936*, 44064*, 44074*, 44104, 44208*, 44227*, 44295*, 44296*, 44297*, 44298*, 44317*, 44368*, 44401*, 44488*, 44521*, 44635*, 44787*, 44820*, 44838*, 44839*, 44840*, 44841*, 44842*, 44843*, 44858*, 45252*, 45463*, 45530*, 45613*, 45858*, 46084*, 46085*, 46086*, 46087*, 46090*, 46395*, 46824*, 46834*, 46837*, 46838*, 46839*, 46929*, 47232*, 47254*, 47301*, 47316*, 47445*, 47939*, 47943*, 48248*, 48249*, 48250*, 48251*, 48253*, 48254*, 48255*, 48256*, 48257*, 48840*, 48841*, 48842*, 48845*, 48871*, 49074*, 49324*, 49392*, 49394*, 49774*, 49775*, 49776*, 49777*, 49778*, 49812*, 49814*, 51076*, 51101*, 51829*, 51830*, 51836*, 51837*, 51842*, 51848*, 51952*, 52423*, 52424*, 52427*, 52946*, 53131*, 53302*, 53347*, 53358*, 53367*, 53368*, 53454*, 53455*, 53456*, 53457*, 53458*, 53459*, 53885*, 53949*, 54022*, 54261, 54398, 54477, 54682*, 54688*, 55134*, 55136*, 55249*, 55250*, 55251*, 55252*, 55254*, 55258*, 55260*, 55566*, 56848*, 56849*, 56850*, 56852*, 56853*, 56854*, 56855*, 56857*, 56859*, 56860*, 56861*, 56862*, 56863*, 56864*, 56865*, 56867*, 56868*, 56870*, 56871*, 56872*, 57319*, 57423, 57536*